arXiv:2611.08487v1 [cs.LG] 5 Nov 2026

User Embeddings are Superpositions of Interpretable Behavioral Modes

Jonathan Kozaczuk **Zheng Dong** **Noyan Evirgen** **Keivan Majidi** **Eddie K. H. Ng**
Chris Porter **Qi Zhao** **Jia Geng** **Changmao Li** **Brandon R. Feng**
Amazon

Abstract

User embeddings are central components of modern recommendation, personalization, and behavioral modeling systems. Though these embeddings can compactly encode rich behavioral information, they are inherently dense and opaque, limiting interpretability. To address this gap, we argue that user embeddings can be understood as sparse superpositions of interpretable behavioral modes. This structure is directly predicted by generative models of user behavior for linear embeddings and extends approximately to deep-learning representations by the superposition hypothesis. Superimposed modes can naturally be recovered by sparse dictionary learning methods, such as sparse autoencoders (SAEs), and recovered modes can be automatically named and queried in natural language. We validate mode recovery against known ground truth on synthetic data, where SAEs recover modes better than classical sparse baselines, including on transformer-encoded embeddings. We then apply the method to classical and transformer-based user embeddings from two real-world datasets. We also show how the corresponding natural-language labels enable zero-shot audience retrieval and characterization over embeddings never trained on text. The framework is post-hoc and model-agnostic, requiring no modification to the upstream embedding system.

1 Introduction

Modern personalization, recommendation, and user-modeling systems aim to understand users and tailor experiences to their preferences. Doing so often relies on representing users in the form of *user embeddings*: dense vectors representing their historical actions and preferences that can be used as input into collaborative filtering or deep learning (DL) models [Raza et al., 2025, Ning et al., 2024]. These embeddings can be generated in a variety of ways, from classical count matrices to transformer-based sequence encoders [Wang et al., 2025].

Although user embeddings can encode rich patterns of user behavior, they are not inherently interpretable. This has several important implications. For example, it is not straightforward to identify *why* a specific recommendation is made for a particular user, or audit what information an embedding contains about a user. It is also not typically possible to query the embedding space using natural language as in text-based semantic search. In this work, we show that the superposition hypothesis from mechanistic interpretability (MI) provides a framework for understanding this opacity and recovering transparent behavioral structure.

A key result in MI is that transformer neurons encode human-interpretable concepts in superposition, recoverable by sparse dictionary methods such as sparse autoencoders (SAEs) and auto-interpretable from activating examples [Bricken et al., 2023, Cunningham et al., 2024]. We argue and empirically demonstrate that user embeddings encode *behavioral modes* in the same way, making them a natural new test case for the MI framework beyond the transformer-residual-stream settings where it was developed. The resulting sparse decomposition yields an interpretable user representation without per-user labeling or text-based embeddings, enabling applications from user insights to natural language semantic search.

40th Conference on Neural Information Processing Systems (NeurIPS 2026).

There are other natural approaches for assigning behavioral modes to users. One can define a taxonomy of modes *a priori* and classify each user into a combination, or prompt an LLM to label each user's interaction history directly. Both approaches require access to raw interaction data and domain-specific configuration, neither operates in the embedding space, and per-user LLM labeling is prohibitively expensive at scale. Our post-hoc decomposition requires only pre-trained embeddings, discovers modes unsupervised from the data, and produces graded mode assignments (e.g., distinguishing a casual from a devoted dog owner) rather than binary labels. It also produces dictionary vectors that support downstream embedding-space operations such as retrieval and audience characterization. We validate this framework on synthetic data with known ground-truth modes, embedded both by mean-pooling and by a trained transformer encoder (mode recovery measured directly), and on two public datasets where zero-shot natural-language audience retrieval over the decomposition serves as an external interpretability test, demonstrating faithful recovery, more behaviorally distinct features than K-Means encoding, and retrieval matching or exceeding classical sparse and text-embedding baselines.

2 Related Work

Sparse autoencoders for embedding interpretability. SAEs were first applied to language model activations to extract monosemantic features from polysemantic neurons [Cunningham et al., 2024, Bricken et al., 2023], and have since been scaled to large frontier models [Gao et al., 2024, Rajamanoharan et al., 2024]. Recent work extends SAEs to *text* embedding spaces [Ye et al., 2024, Park et al., 2025, Kang et al., 2025, Jiang et al., 2025] and to non-LLM embeddings in other domains including speaker, pathology, cell-image, radiology, and CLIP representations [Pluth et al., 2025, Le et al., 2024, Dasdelen et al., 2025, Abdulaal et al., 2024, Zaigrajew et al., 2025]. These methods all ground latents in semantics available in the input modality (text tokens, images, audio frames). Our work extends SAE decomposition to *behavioral* embeddings that encode non-textual interaction sequences, requiring a different interpretation pipeline and enabling natural language semantic search over embedding spaces that were never trained on text.

SAEs for recommender systems. Two concurrent works apply SAEs in recommender settings. Spíšák et al. [2026] insert an SAE between the encoder and decoder of a collaborative filtering autoencoder, and Klenitskiy et al. [2025] apply SAEs to the hidden states of transformer-based sequential recommenders. Both target recommendation steering or control. Our work differs in that we decompose pre-trained user embeddings post-hoc without modifying the recommendation model, evaluate against known ground-truth behavioral modes, and validate interpretability of the decomposition directly on audience understanding and natural-language semantic search.

Criticism of SAEs and random baselines. Korznikov et al. [2026] show that SAEs with frozen-random decoders can match fully trained SAEs in high-dimensional LLM residual streams at high overcompleteness, and Cui et al. [2026] further demonstrates SAEs can fail to recover ground-truth LLM features. We directly address these concerns in Section 4 by comparing against the soft-frozen-decoder baseline of [Korznikov et al., 2026] on our synthetic setup, where the ground-truth modes allow a direct measurement of per-user mixture-weight recovery. This equivalence does not hold at moderate overcompleteness (Section 4).

User-representation decomposition and disentanglement. Prior work on interpreting user representations takes two approaches. *End-to-end disentanglement*, as in MacridVAE and DisenHAN [Ma et al., 2019, Wang et al., 2020, Zheng et al., 2021, Fang et al., 2025], incorporates disentanglement objectives into the upstream recommender at training time. *Post-hoc decomposition* applies unsupervised dictionary learning to pre-trained representations. Classical post-hoc methods include NMF, PCA, Archetypal Analysis, and k-means for behavior segmentation [Drachen et al., 2013], and topic models (LDA and extensions) which treat interactions as words drawn from latent topics and produce interpretable topics [Mukherjee et al., 2017, Chaudhuri et al., 2021]. We take the post-hoc approach. In contrast to topic models, which operate on raw interactions, our method decomposes pre-trained user embeddings directly, leveraging the richer behavioral signal they encode (e.g., co-viewing sequence, rating intensity, genre co-occurrence) beyond what simple interaction counts capture. Our contribution includes the MI-grounded framework for analyzing user embeddings as sparse superpositions of behavioral concepts, allowing us to recover and identify behavioral modes in natural language. This enables zero-shot natural-language audience retrieval from the recovered modes.

Audience retrieval. The standard approach to audience retrieval is *lookalike modeling*: given a seed set of example users, find similar users in an embedding space [Liu et al., 2019, Zhu et al., 2021, Peng et al., 2023, Wei et al., 2024]. These methods require pre-defined example users ("seeds") and provide no transparency into what behavioral patterns drive the retrieved audience. Our method queries over automatically interpreted sparse behavioral modes, requiring neither seed users nor text-aligned training data.

3 Superposition from a generative model of user behavior

In this section, we analyze a simple generative model for user behavior to motivate why and how superposition arises in user embeddings. The derivation is exact in expectation for embedding functions that average per-observation features, and serves as a plausibility argument for deep-learning encoders via the superposition hypothesis, which we test empirically for transformer encoders in Sections 4 and 5 below. Consider a user $\mathcal{U}$ interacting in a specific environment $\mathcal{W}$, where each interaction produces an observation $\mathbf{z} = (z_1, \ldots, z_N)$ comprising N observable features. A given user's behavior in $\mathcal{W}$ is summarized as a matrix $H_{\mathcal{U}}$, where $(H_{\mathcal{U}})_{ij} = z_j(\mathcal{U}; t_i)$, the observed feature value for $\mathcal{U}$ at interaction t_i. Here t_i labels a particular interaction of $\mathcal{U}$ with the environment. Note that $H_{\mathcal{U}}$ is implicitly time-dependent, since a user's interactions with the environment are dynamic. We will suppress time dependence throughout this study for simplicity, but at any given snapshot our methodology will apply.

We assume there exist a discrete set of *behavioral modes*, $\{\mathcal{P}_k \mid k = 1, \ldots, K\}$, which are interpretable user types with associated distributions $p_k(\mathbf{z})$ that define the mode's behavior patterns. Modes can be defined at arbitrary granularity: one can always merge two modes into one or split a mode into finer sub-modes. Examples of behavioral modes might be dog lovers on a shopping platform, binge-watchers on a streaming service, or commute-dominated mobility patterns in a ride-sharing app. We further assume each user's behavior is governed by a sparse subset of modes, with user-specific non-negative weights $\mathbf{w} \in \mathbb{R}^K_{\geq 0}$, $\|\mathbf{w}\|_0 \ll K$, $\sum_k w_k = 1$. Conditioned on $\mathbf{w}$, each interaction for a user $\mathcal{U}$ is drawn independently from the mixture

$$p_{\mathcal{U}}(\mathbf{z}) = \sum_{k=1}^{K} w_k \, p_k(\mathbf{z}). \tag{1}$$

The weight vector $\mathbf{w}$ captures both which modes are active and their relative prevalence in the user's behavior. Equation (1) is a mixed-membership model: each user belongs to multiple modes simultaneously, with each interaction generated by one mode. When the observations are discrete (e.g., individual product purchases treated as tokens), this reduces to the Latent Dirichlet Allocation (LDA) generative model [Blei et al., 2003], with behavioral modes playing the role of topics and products playing the role of words. Our formulation generalizes this to continuous and vector-valued observations, but inherits the same core structure: a population of users, a shared set of latent modes, and sparse per-user mixtures.

3.1 Superposition in embedding space

A user embedding $\mathbf{u}$ for user $\mathcal{U}$ is defined by $\mathbf{u} = F(H_{\mathcal{U}})$, with $F : \mathbb{R}^{T_{\mathcal{U}} \times N} \to \mathbb{R}^m$, where $T_{\mathcal{U}}$ is the user's number of interactions (variable across users), m is the embedding dimension, and typically $m \ll N$. Common examples of F include classical embedding models (e.g., SVD on a counts matrix) or neural networks (e.g., behavioral sequence encoders).

A key consequence of the generative model in Eq. (1) is that when F is a sample mean of per-observation features f (as with mean-pooled product embeddings), the user embedding inherits a sparse superposition structure in expectation:

$$\mathbf{u} \approx \sum_{k=1}^{K} w_k \, \mathbf{d}_k, \qquad \text{where} \quad \mathbf{d}_k \equiv \mathbb{E}_{z \sim p_k}[f(z)] \tag{2}$$

is the expected embedding of observations drawn purely from mode k and $f : \mathbb{R}^N \to \mathbb{R}^m$ maps individual observations to their embeddings. User embeddings are therefore sparse linear superpositions of *mode centroids* $\mathbf{d}_k$. Analogous expressions hold for linearly-transformed sample-mean

pooling, $F = A \cdot \frac{1}{T_u} \sum_i f(\mathbf{z}_i)$ for a fixed matrix A (e.g., a projection), with the centroids replaced by their images $A\mathbf{d}_k$. These centroids need not be orthogonal: modes with overlapping observation distributions (e.g., "coffee connoisseur" and "home barista") produce correlated directions, and when $m < K$ even unrelated modes must share them. Both effects place the centroids in *superposition* in the sense of [Elhage et al., 2022], motivating the use of overcomplete sparse dictionaries rather than orthogonal decompositions for recovery.

Embeddings from *nonlinear* deep-learning encoders admit a similar structure, which we illustrate via the transformer case. Under the superposition hypothesis [Elhage et al., 2022], each residual-stream position satisfies $\mathbf{r}_\ell \approx \sum_j a_j^{(\ell)} \mathbf{d}_j$. For a user embedding formed by any linear pooling of positions (mean-pool, sum-pool), linearity gives $\mathbf{u} \approx \sum_j \tilde{a}_j \mathbf{d}_j$ with $\tilde{a}_j$ the matching linear combination of $\{a_j^{(\ell)}\}_\ell$. A mode $\mathcal{P}_k$ induces a distribution over observations and hence over transformer features. If the expected activations decompose linearly in the mode mix $\mathbf{w}$, the feature directions sum into a mode-level centroid $\tilde{\mathbf{d}}_k = \sum_j \mathbb{E}_{p_k}[\tilde{a}_j]\, \mathbf{d}_j$ replacing $\mathbf{d}_k$ in Eq. (2), where the expectation is over histories with interactions drawn from p_k. An SAE applied to pooled embeddings therefore recovers mode-level structure rather than individual transformer features. For single-position readouts (last-token, [CLS]) the linear-pooling argument does not apply directly. We conjecture that behavioral-mode resolution emerges from training dynamics, since the objective depends on aggregate sequence structure rather than individual items, but leave verification to future work. Our experiments mean-pool across final-layer positions, so the analysis above applies directly. When attention contextualizes interactions so the linearity-in-$\mathbf{w}$ assumption fails, SAE latents may correspond to finer or composite structure rather than aligning one-to-one with the ground-truth $\mathcal{P}_k$. Since modes admit arbitrary granularity (Section 3), the recovered latents remain behavioral modes, at a granularity shaped by the encoder rather than fixed by the generative model.

Under the flat generative model of Eq. (1) with sample-mean F, each $\mathcal{P}_k$ contributes a single direction $\mathbf{d}_k$, so any further splitting of $\mathbf{d}_k$ across multiple SAE latents is artifactual *feature splitting* [Bricken et al., 2023, Templeton et al., 2024, Chanin et al., 2024]. At the single-example level the L_1 penalty favors a single aligned atom, but over a population of users the penalty can prefer finer-grained atoms that each activate on a distinct subset of users, reducing the total L_1 mass under overcompleteness. Split features can be identified by decoder-direction similarity or correlated activations across users and merged post-hoc, which we validate on synthetic data in Section 4. For nonlinear F, the previous paragraph identified an additional source of finer-grained latents from attention-driven context-dependence, and merging absorbs only the artifactual-splitting component.

3.2 Recovery via sparse autoencoders

Equation (2) implies that recovering behavioral modes from a population of user embeddings is a sparse dictionary learning problem: given $\{\mathbf{u}_i\}_{i=1}^M$, find a dictionary $D \in \mathbb{R}^{m \times d_{\text{hidden}}}$ and sparse non-negative codes $\{\hat{\mathbf{w}}_i\}$ such that $\mathbf{u}_i \approx D\hat{\mathbf{w}}_i$. The SAE's dictionary width d_{hidden} is typically larger than the embedding dimension m to accommodate superposition, and need not equal the ground-truth mode count K.

This problem has classical solutions in the discrete observation domain: LDA recovers topics from token counts via variational inference, and NMF recovers non-negative factors from count matrices. However, these methods require access to the raw interaction data and cannot leverage the semantic geometry captured by modern embedding models. We instead operate directly on embeddings using sparse autoencoders (SAEs), which learn a sparse dictionary representation of the input with sparsity enforced by an L_1 penalty on encoder activations. In particular, the "vanilla" ReLU SAE is defined on an input embedding $\mathbf{u}$ as

$$\hat{\mathbf{u}} = W_{\text{dec}}\ \text{ReLU}(W_{\text{enc}}\,\mathbf{u} + \mathbf{b}). \tag{3}$$

In terms of Eq. (2), the j-th SAE latent estimates a mode weight and its decoder column estimates the mode direction:

$$\hat{w}_j \equiv \text{ReLU}(W_{\text{enc}}\,\mathbf{u} + \mathbf{b})_j, \qquad (\hat{\mathbf{d}}_j)_\ell \equiv (W_{\text{dec}})_{\ell j}, \quad j = 1, \ldots, d_{\text{hidden}}. \tag{4}$$

The SAE is trained to minimize $\mathcal{L}(\mathbf{u}) = \|\hat{\mathbf{u}} - \mathbf{u}\|_2^2 + \lambda \sum_{j=1}^{d_{\text{hidden}}} \hat{w}_j$, where the sparsity term drops the absolute value since $\hat{w}_j \geq 0$ after the ReLU. The decoder columns are unit-normalized so that they constitute unit vectors in the original embedding space.

Typically in mechanistic interpretability work, the SAE is *overcomplete*, with the hidden dimension larger than the input dimension ($d_{\text{hidden}} > m$), so that superposition can be disentangled. For user embeddings, the number of behavioral modes K may be less than the embedding dimension m, however the individual $\mathbf{d}_k$ are still typically in superposition and non-orthogonal. The relevant overcomplete regime in our case is therefore d_{hidden} large enough that the SAE can dedicate features to each mode, or to each sub-mode in the case of nonlinear encoders where behavioral modes split into finer directions. Note that this is not possible with techniques such as PCA, whose components are orthogonal by construction. We compare SAEs against classical sparse dictionary baselines including sparsified versions of PCA, ICA, NMF, and K-Means encoding in our experiments below. Each baseline captures part of the mode structure assumed by Eq. (2) but lacks at least one key property: overcompleteness (PCA/ICA), the ability to handle signed input (NMF), or the freedom for dictionary directions to point beyond cluster centers (k-means encoding).

Provided the SAE recovers the underlying behavioral modes, its latents should have interpretable descriptions recoverable from the data. We obtain these via auto-interpretation [Bricken et al., 2023, Cunningham et al., 2024]: for each SAE latent we pass activating and non-activating user examples with their interaction histories to an LLM and prompt it to identify the dominant pattern in the positives. The output is a set of empirical latents $\{\hat{\mathcal{P}}_k\}$, each comprising a name $\hat{\mathcal{N}}_k$, description $\hat{\mathcal{D}}_k$, and basis vector $\hat{\mathbf{d}}_k$ in the original embedding space. This enables decomposing audiences in terms of behavioral modes and natural-language semantic search by selecting codes with highest semantic overlap with a query and retrieving users with the highest activations on those codes. The same auto-interpretation step can be applied to the classical sparse baselines. Additionally, the LLM outputs a confidence score alongside each name. Because the name and description are grounded in the vocabulary shown to the LLM (e.g., item titles, categories), latents whose defining axis falls outside that vocabulary receive lower confidence. These are typically finer-grained features in the nonlinear-F regime. We expect such latents to remain monosemantic and interpretable under a richer vocabulary, but we gate on confidence ≥ 0.6 at retrieval to keep named features within the vocabulary's resolution.

4 Experiments on Synthetic Data

Assuming behavioral mode superposition in embedding space, to what extent can SAEs and other methods faithfully recover behavioral modes under controlled conditions where the ground truth is known? That the embedding of a sparse mixture is a sparse combination of mode centroids follows from Eq. (2). However, it is *not* guaranteed that these centroids can be recovered from the embeddings alone. To test this, we construct synthetic user embeddings with known mode mixtures, apply the SAE, and measure whether its latents correspond to the true modes (no auto-interpretation is needed, since the ground truth is known). This validates recovery under the framework's assumptions. Whether user embeddings extracted from real-world datasets exhibit the assumed structure is tested in Section 5. Classical baselines (PCA, ICA, K-Means encoding, NMF) test whether the structural constraints identified in Section 3.2 (enforced orthogonality, non-negative input, cluster-centered directions) bottleneck mode recovery.

Setup. We define $K=75$ behavioral modes (e.g., "dog lover", "new parent"), each with a description and example products. Each of 100,000 synthetic users is assigned 2 to 6 active modes, chosen in proportion to mode popularity, with log-normal mixture weights (e.g., 0.7×"dog lover" + 0.3×"new parent"). We prompt Claude Sonnet 4 to write a purchase history for each user (median 55 orders) whose interactions follow these weights, plus 5 to 20% off-mode noise (see Appendix A). We chose $K=75$ so that the embedding dimensions swept below ($m = 16$ to 128) bracket the mode count. Item popularity is heavy-tailed, with the top 1% of items carrying 51% of interactions. We embed each product with `all-mpnet-base-v2` and mean-pool over the user's interactions, yielding a 768-dimensional embedding that is a superposition of the underlying modes. To further vary the amount of superposition, we follow the techniques in [Bingham and Mannila, 2001] and project these embeddings onto random directions in $\mathbb{R}^m$. The dimension m is varied across the experiment. Finally, the embeddings are standardized and L_2-normalized.

We train an SAE with $d_{\text{hidden}} = 300$ (4× overcomplete relative to ground truth) with an adaptive sparsity penalty ensuring that the mean number of active latents (L_0) matches the ground-truth mean number of modes per user. We compare against six baselines: random projections onto 300 unit

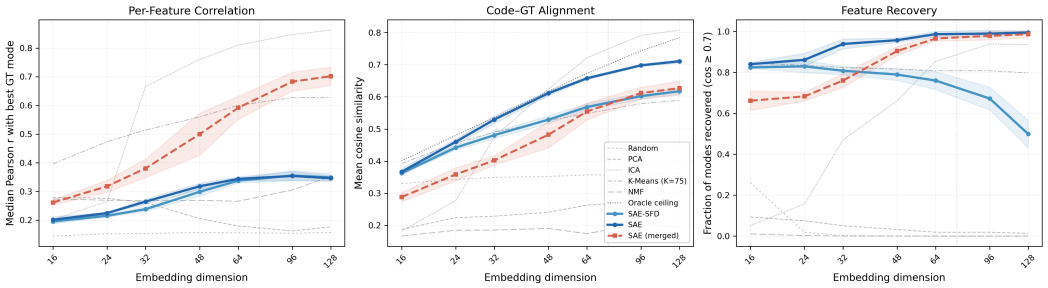


Figure 1: Mode recovery vs. embedding dimension m (mean $\pm$ 1 std over 5 random projections). Left: median per-feature Pearson r with best-matching ground-truth mode. Center: mean per-user cosine similarity between projected codes and ground-truth weight vector. Right: fraction of modes recovered at decoder–centroid cosine similarity ≥ 0.7. The vertical line marks $m = 75$, the ground-truth mode count.

vectors with ReLU, sparsified versions of PCA and FastICA, *K-Means encoding* (cosine similarity to K-Means centroids passed through ReLU and thresholded to match the SAE's L_0, following [Coates and Ng, 2012]), the soft-frozen decoder SAE of [Korznikov et al., 2026], and NMF on shifted (non-negative) embeddings. Matching the ground-truth mode count, K-Means encoding uses 75 components, and PCA, ICA, and NMF use $\min(75, m)$. NMF keeps its natural sparsity (no post-hoc thresholding). K-Means is additionally evaluated with 512 components to isolate raw capacity from decomposition quality. Further details are in Appendix A.

To measure ground truth recovery, each component is matched to its best ground-truth mode by Pearson correlation between component activations and mode weights across users. This mapping is many-to-one: when multiple components map to the same mode, their activations are summed. We also report SAE results after merging features whose decoder directions have cosine similarity > 0.45.

Results. We evaluate three metrics (Fig. 1, all at matched L_0): *per-feature correlation* (Pearson r between each component and its best-matching mode), *code–GT alignment* (per-user cosine similarity after mapping components to modes), and *feature recovery* (fraction of modes with a decoder direction at cosine ≥ 0.7). An oracle ceiling (least-squares from projected embeddings to ground-truth weights) bounds what any linear method can achieve at each m.

In the high-superposition regime $m < K = 75$, the SAE matches or exceeds every classical baseline in Fig. 1 on mode recovery and stays close to the oracle ceiling on code–GT alignment. K-Means encoding holds steady near 80% recovery (tied with the SAE at $m = 16$) and matches or slightly exceeds the SAE on alignment at $m \leq 24$. PCA recovers almost no modes at any m ($\leq 9\%$), as expected since its orthogonal components cannot align with non-orthogonal mode centroids. FastICA overtakes the SAE on alignment from $m = 48$ but recovers fewer modes at cosine ≥ 0.7 (Fig. 1). K-Means with a 512-component dictionary (not shown in Fig. 1) recovers more mode directions than the SAE at $m \leq 48$ but does not close the alignment gap: it underperforms the 75-component reference at every $m \geq 32$ on code–GT alignment (paired Wilcoxon $p \approx 0.03$ at $m \geq 48$), so added capacity alone does not give K-Means the SAE's per-user weight recovery. The soft-frozen decoder SAE of [Korznikov et al., 2026], their strongest baseline for feature recovery, tracks the SAE only at low m where our setup enters Korznikov's high-overcompleteness regime ($d_{\text{hidden}}/m \gg 1$). Our real-data experiments sit at $d_{\text{hidden}}/m = 4$ and omit this baseline. Frozen-encoder and frozen-decoder variants each fail on routing or direction recovery respectively outside this regime [Korznikov et al., 2026], so training both components is load-bearing at our overcompleteness.

Per-feature correlation reveals the feature splitting discussed in Section 3.1: raw SAE median $r \approx 0.35$ rises to ≈ 0.70 at m=128 after merging, confirming the splitting is artifactual. With ground truth known, we can also analyze how monosemantic each feature is: for each mode we identify the feature that best ranks mode-positive users above mode-negative users (Precision among the top n_{pos}), and report the mean across modes. The merged SAE produces 1.4–$2\times$ more monosemantic latents than K-Means encoding or raw embedding dimensions (0.53 vs. 0.39 and 0.28 at m=128, using a separately trained 512-wide SAE on one projection). FastICA attains even higher per-feature monosemanticity (0.75) since the generative model's independent-mode assumption exactly matches its objective, but with lower decoder-direction recovery at high cos thresholds (Fig. 1).

Transformer embeddings. Eq. (2) holds only approximately for nonlinear encoders (see Section 3.1), so we repeat the experiment on embeddings from a trained sequence encoder: SASRec with the architecture and hyperparameters of our MovieLens encoder (see Appendix E.1), trained on the synthetic interaction sequences and mean-pooled into $d{=}256$ user embeddings (see Appendix A.6). The oracle ceiling stays close to that of the mean-pooled product embeddings at the same dimension (0.78 vs. 0.85). The SAE leads every method on code–GT alignment (0.58, vs. 0.53 for FastICA, 0.45 for K-Means encoding, 0.37 for LDA fit to the raw user–item counts, and 0.25 for PCA) and recovers 73 of 75 modes at cosine ≥ 0.7, close to its 100% on the mean-pooled embeddings, while FastICA and K-Means encoding drop from 95% to 59% and from 79% to 52%. The SAE also recovers more modes than PCA, FastICA, and K-Means encoding at every projected dimension $m \in [16, 128]$, keeps the best alignment when the encoder itself is trained at $d{=}64 < K$, and captures a nearly constant 73–75% of the oracle ceiling as the number of modes varies from 15 to 75 (see Appendix A.6).

5 Behavioral Modes in Real World Data

We evaluate on two complementary datasets: `Open e-commerce 1.0` [Berke et al., 2024] (1.8M purchases from 5027 U.S. consumers, with a self-reported life-event survey) and MovieLens 1M [Harper and Konstan, 2015] (1M ratings, 6040 users, 3706 movies). We use the same pipeline on both: generate user embeddings (method-specific, described in each subsection), train a sparse decomposition, and auto-interpret each latent with an LLM from its top-activating users. At query time, the feature interpretations are shown to an LLM alongside a natural-language audience query. The LLM scores each latent's relevance on a 0–10 scale and we retain features scoring ≥ 5. Users are then ranked by the weighted sum of their activations on the retained features. We use Claude Sonnet 4.6 for interpretation and Claude Haiku 4.5 for query-time feature scoring. Replacing the interpretation model with the open-weight Llama 3.3 70B on one Open e-commerce seed leaves SAE retrieval largely unchanged and keeps the SAE ahead of every baseline on mean Lift, with narrower margins over FastICA and K-Means encoding (see Appendix C.5).

Our primary method is a ReLU SAE with fixed L1 sparsity penalty and $4\times$ overcompleteness (width chosen per embedding, sparsity λ selected via the decoder-orthogonality criterion of [Chanin and Garriga-Alonso, 2025]).[1] As classical sparse alternatives we report ***K-Means encoding*** (defined in Section 4) and FastICA (the most competitive classical baseline on Open e-commerce), with PCA in Appendix B. We also report a ***text-embedding baseline*** as the natural zero-shot NL-retrieval alternative that requires no decomposition: we embed a per-user text summary and the NL query with `all-MiniLM-L6-v2` and rank by cosine similarity. The summary is a TF-IDF-weighted mean of sentence-transformer embeddings over purchased category names for Open e-commerce (matching the exact signal the SAE, K-Means, and ICA consume) and the mean of watched movie-title embeddings for MovieLens. For each task we report Lift@n_{pos}, AUROC, Coverage (fraction of positives with nonzero retrieval score), and FVU (fraction of embedding variance unexplained by the best linear decoder fit from the method's codes); Lift, AUROC, and Coverage are averaged across tasks.

5.1 Open e-commerce

Setup. We segment user order histories into 6-month windows, build per-window user-by-category count matrices over the 1864 categories with more than 5 purchases in any window, apply log scaling and TF-IDF weighting, L_2-normalize each row, and take truncated SVD to 128 dimensions. Apart from the log scaling and row normalization this embedding is linear in the category counts, so its structure approximately matches Eq. (2). The SAE is $4\times$ overcomplete ($d_{\text{hidden}}{=}512$) with mean $L_0{\approx}23$ (Appendix C). Tasks split into (i) *category retrieval* (6 tasks spanning base rates 8 to 54%: pet owner, coffee enthusiast, gardener, board gamer, baby products, musician), where positives are users who purchased in the target categories in post-2021 windows, and (ii) *life-event retrieval* (new parent, moved residence), where positives are users who self-reported the life event in 2021.

Results. SAE decomposition recovers the underlying behavioral modes faithfully enough to support zero-shot natural-language retrieval that matches or exceeds every classical sparse baseline on every

[1] MovieLens embeddings are L_2-normalized and then standardized before SAE training, and Open e-commerce embeddings are used as produced. These steps preserve the form of Eq. (2) up to a per-user rescaling of the mode weights, a fixed linear map of the centroids, and a constant offset.

Table 1: Open e-commerce zero-shot NL audience retrieval, metrics averaged per task block (6 category tasks and 2 life-event tasks, see Appendix C.2). $\text{AUROC}_{\text{scored}}$ restricts AUROC to users with nonzero scores. Text baseline is the matched-input category-pooled variant (Section 5). Text baseline has no FVU.

Task type	Method	FVU ↓	Lift	AUROC	$\text{AUROC}_{\text{scored}}$	Coverage
Category	SAE (ours)	**0.075**	**1.93**×	**0.705**	**0.678**	0.735
	FastICA	0.083	1.86×	0.695	0.660	**0.770**
	K-Means encoding	0.388	1.85×	0.680	0.663	0.614
	Text-embedding baseline	—	1.39×	0.633	0.633	1.000
Life-event	SAE (ours)	**0.075**	**5.30**×	0.715	**0.741**	0.876
	FastICA	0.083	4.75×	0.713	0.717	**0.932**
	K-Means encoding	0.388	4.29×	0.676	0.693	0.738
	Text-embedding baseline	—	2.13×	0.636	0.636	1.000

Table 2: MovieLens zero-shot NL audience retrieval, averaged over 2 SAE-training seeds × 32 non-compositional queries (query list in Appendix E.2). FVU is from a single SAE seed per encoder. Text baseline is encoder-independent. Bold: SAE significantly better than K-Means encoding ($p<0.05$, cross-seed paired Wilcoxon, see Appendix D).

Encoder	Method	FVU ↓	Lift	AUROC	$\text{AUROC}_{\text{scored}}$	Coverage
SASRec	SAE (ours)	0.041	2.53	0.692	**0.687**	**0.977**
	K-Means encoding	0.136	2.16	0.678	0.663	0.811
BERT4Rec	SAE (ours)	0.032	2.38	0.690	0.688	**0.984**
	K-Means encoding	0.108	2.41	0.697	0.676	0.848
—	Text-embedding baseline	—	1.64	0.701	0.701	1.000

retrieval-quality metric. SAE significantly exceeds K-Means encoding on every metric across both task blocks (cross-seed paired Wilcoxon, 5 seeds: all $p \leq 0.009$; Appendix D) and PCA on every metric (all $p<10^{-3}$). FastICA is the closest competitor: on category tasks SAE wins Lift ($p=2\times10^{-4}$), AUROC ($p=0.004$), and $\text{AUROC}_{\text{scored}}$ ($p=3\times10^{-4}$); on life-event tasks SAE wins Lift and $\text{AUROC}_{\text{scored}}$ ($p=0.001$ each) and ties on AUROC ($p=0.5$, 0.715 vs. 0.713). ICA is higher on Coverage across both blocks (due to its denser activations). Against the text-embedding baseline, SAE wins on Lift and AUROC (Coverage is not a meaningful axis for this similarity-search baseline). SAE and ICA have the highest reconstruction fidelity (FVU 0.075 vs. 0.083); PCA and K-Means lag (0.36–0.39). Note that reconstruction quality does not always translate to retrieval performance: ICA matches SAE on FVU but trails on Lift (Table 8).

5.2 MovieLens 1M

Setup. MovieLens 1M tests the *nonlinear* transformer-embedding regime where the superposition of Eq. (2) holds only approximately (see Section 3.1). To test encoder-architecture robustness we train two transformer recommenders on chronologically ordered interactions: **SASRec** [Kang and McAuley, 2018] (causal self-attention, next-item prediction) and **BERT4Rec** [Sun et al., 2019] (bidirectional self-attention, masked-item Cloze), both at $d_{\text{model}}=256$ with user embeddings obtained by mean-pooling final-layer hidden states. The SAE is $4\times$ overcomplete ($d_{\text{hidden}}=1024$) with mean $L_0 \approx 80$. Full SAE and transformer hyperparameters are in Appendix E.1. The decoder-orthogonality operating point (see Section 5) minimizes artifactual feature splitting in-training, so no post-hoc merging is applied on real data. Residual finer-grained latents under nonlinear F are implicitly handled via the auto-interp confidence filter at retrieval (see Section 3.2). Features that track engagement intensity rather than taste are identified and relabeled as engagement-axis features before retrieval, uniformly across SAE and K-Means-encoding codes (Appendix E.6). We evaluate on 32 natural-language audience queries (21 broad, 11 niche, full list in Appendix E.2). Ground truth is generated by a deterministic title-pattern rule: for each query we curate a list of matching movie titles from the MovieLens catalog, optionally gated by a MovieLens genre constraint, and label a user positive if their watch history contains ≥ 3 such titles.

Results. At matched dictionary size ($d_{\text{hidden}}=1024$) and matched L_0, SAE decomposition and K-Means encoding are matched on Lift and AUROC (cross-seed paired Wilcoxon $p \geq 0.1$ on both encoders; Table 10). The SAE advantage is structural, and surfaces on three axes: *coverage* (98% vs.

K-Means encoding top-5 for Jurassic Park *5/5 paraphrase a comedy concept*		**SAE (ours) top-5 for Jurassic Park** *5 distinct concepts*	
COMEDY	Late-1990s indie/quirky dramedies	THRILLER	1990s B-movie action-thriller
COMEDY	Early-2000s indie/quirky comedy	ACTION	Low-quality 1990s action blockbuster
COMEDY	Low-budget 1990s B-movie comedy	COMEDY	1990s low-quality mainstream comedy
COMEDY	1990s low-quality mainstream comedy	SEQUEL	1980s-90s action-comedy sequel
COMEDY	LGBT romantic comedy and drama	SCI-FI	1990s B-grade sci-fi action

Figure 2: Top-5 features describing the Jurassic Park audience (a sci-fi action franchise) under K-Means encoding and SAE on SASRec, ranked by lift at a 10% top-activator threshold. All five K-Means features paraphrase a mainstream-comedy concept, while the SAE top-5 span five distinct themes. Small-caps tags are our one-word summaries of the LLM-assigned feature names.

81–85% of true positives scored, $p<10^{-4}$ on both encoders), *scored ranking* (higher $\text{AUROC}_{\text{scored}}$ on SASRec, $p=0.014$, trending on BERT4Rec, $p=0.07$), and *reconstruction fidelity* (96–97% of embedding variance recovered from SAE codes vs. 86–89% from K-Means codes). The text-embedding baseline reaches 100% coverage by construction (it embeds every user's watched-title history densely) and a comparable AUROC. Its Lift, which measures precision at the top of the ranking, is significantly below the SAE's on both encoders (Stouffer $p<10^{-3}$). These results are consistent across both transformer objectives (causal next-item and bidirectional masked). Because MovieLens ground truth is derived from titles, we also retrieve against 14 held-out self-reported demographic labels that no stage of the pipeline sees. The text-embedding baseline, which matched the SAE on AUROC for the title-derived tasks, falls to near-chance AUROC, significantly below the SAE, and its Lift remains well below the SAE's (see Appendix E.3). The coverage advantage holds, and the Lift and AUROC differences with K-Means encoding stay small, at every auto-interpretation confidence threshold from 0.0 to 0.7 (see Appendix E.4).

The central MovieLens finding is not that SAE ranks better than K-Means. K-Means encoding is itself a sparse decomposition, and it retrieves competitively because the superposition structure is there for its centroids to approximate. At matched dictionary size and sparsity both methods saturate the same ranking signal, and the finding is *structural*: the SAE dictionary is near-orthogonal (pairwise decoder cosines centered at 0, mean absolute value 0.06 to 0.08 on SASRec), while K-Means centroids overlap (mean pairwise cosine 0.29 on SASRec, 0.17 on BERT4Rec, see Appendix E.1) and multiple centroids partition the same neighborhood. Overlapping centroids paraphrase one region of the embedding space and leave others uncovered, which costs coverage before it costs rank order, and the same geometry drives the feature-level redundancy in Section 5.3. On Open e-commerce, whose embedding is approximately linear, the same comparison favors the SAE on every retrieval metric (see Section 5.1). On broad queries against a saturated ranking signal, we do not expect ranking gains from orthogonality alone.

5.3 Audience characterization

A second application of the decomposition is *audience characterization*: given a behaviorally-defined audience, surface the features that best describe it. A useful top-k feature set should span *distinct* explanatory concepts rather than paraphrase a single concept, and should cover the target audience under semantically-grounded selection. On 20 franchise-level audiences in MovieLens-1M at $k=5$, the SAE top-k features are significantly less redundant than the matched-L_0 K-Means-encoding top-k (Stouffer $p\approx 4\times10^{-4}$) and cover significantly more of the target audience under reverse-selector ranking (Stouffer $p\approx10^{-7}$, see Appendix D). Within confidence-filtered features (≥ 0.6) that surface the same niche audience, K-Means encoding allocates $2.2\times$ more features per distinct concept than SAE (2.20 vs 1.00 redundancy ratio, averaged across 5 niche audiences; Appendix E.5). The effect is even more pronounced on Open e-commerce's approximately linear embeddings (2.82 vs 1.14, or $2.5\times$, see Appendix E.5), as anticipated by our generative framework. The K-Means reference has higher per-feature lift but narrower per-feature activation distributions, so its redundant top-k does not translate into better audience coverage. Figure 2 illustrates on the Jurassic Park audience. See Appendix E.5 for the full protocol and the reverse-selector definition.

6 Conclusion

In this work, we extended the superposition hypothesis for learned representations to user embeddings, arguing that both classical (linear) and deep-learning user embeddings decompose into sparse superpositions of interpretable behavioral modes recoverable by sparse autoencoders. Empirical feature-level analysis supports the framework: for both transformer encoders on MovieLens, SAE decompositions produce more behaviorally distinct features than the strongest classical baseline. On synthetic data, SAEs recover more known ground-truth modes than classical decomposition methods, and this holds for transformer-encoded embeddings as well. On the mean-pooled synthetic embeddings, a fixed post-hoc merging procedure approximately restores the mode granularity assumed by the generative model despite overcomplete feature splitting. On two real-world datasets, the resulting decompositions enabled natural-language audience retrieval over embeddings never trained on text. Because the method is post-hoc and model-agnostic, it applies to any pre-trained embedding without modifying the upstream system.

More broadly, behavioral mode decomposition provides a general-purpose lens for understanding what user embeddings encode. This has practical implications for auditing recommendation systems, surfacing what behavioral signals drive personalization, and giving practitioners transparent, queryable representations of their user base. The same capability carries privacy risk. Making an embedding queryable in natural language lowers the cost of inferring sensitive traits, such as recent life events, and extends it to anyone holding the embeddings and the interaction histories of the example users shown during interpretation. Because the recovered features are enumerable and named, sensitive directions can also be detected, excluded, or ablated, which is not possible with a dense embedding.

Several extensions remain open. We considered at most two temporal snapshots per user, but behavioral modes evolve, and their temporal dynamics may signal shifts in preference or life circumstance. Our weighted-sum combinator handles additive concept overlap but not logical constraints or temporal sequencing (e.g., "viewers who shifted from A to B"). Explicit combinators over mode directions are a natural next step. We also experimented only with ReLU SAEs, and other SAE variants and sparse dictionary learning algorithms remain to be tested. Both real-world datasets represent consumption domains with positive-only interaction sequences, and both deep encoders are transformer sequential recommenders (SASRec, BERT4Rec). Domains with different interaction semantics (e.g., mobility or explicit negative feedback) and other deep-learning architectures (e.g., MLP or CNN encoders) remain to be tested. Finally, recent work identifies persona-like structure in LLM internal states via linear probing [Chen et al., 2025, Lu et al., 2026]. Our results suggest SAE-based recovery may discover richer persona structure post-hoc, particularly when persona directions are non-orthogonal or overcomplete.

References

Ahmed Abdulaal, Hugo Fry, Nina Montaña-Brown, Ayodeji Ijishakin, Jack Gao, Stephanie Hyland, Daniel C. Alexander, and Daniel C. Castro. An X-ray is worth 15 features: Sparse autoencoders for interpretable radiology report generation. *arXiv preprint arXiv:2410.03334*, 2024.

Alex Berke, Dan Calacci, Robert Mahari, Takahiro Yabe, Kent Larson, and Sandy Pentland. Open e-commerce 1.0, five years of crowdsourced u.s. amazon purchase histories with user demographics. *Scientific Data*, 11(1):491, May 2024. doi: 10.1038/s41597-024-03329-6. URL `https://doi.org/10.1038/s41597-024-03329-6`.

Ella Bingham and Heikki Mannila. Random projection in dimensionality reduction: applications to image and text data. In *Proceedings of the Seventh ACM SIGKDD International Conference on Knowledge Discovery and Data Mining*, KDD '01, page 245–250, New York, NY, USA, 2001. Association for Computing Machinery. ISBN 158113391X. doi: 10.1145/502512.502546. URL `https://doi.org/10.1145/502512.502546`.

David M. Blei, Andrew Y. Ng, and Michael I. Jordan. Latent Dirichlet allocation. *Journal of Machine Learning Research*, 3:993–1022, 2003.

Trenton Bricken, Adly Templeton, Joshua Batson, Brian Chen, Adam Jermyn, Tom Conerly, Nick Turner, Cem Anil, Carson Denison, Amanda Askell, Robert Lasenby, Yifan Wu, Shauna Kravec,

Nicholas Schiefer, Tim Maxwell, Nicholas Joseph, Zac Hatfield-Dodds, Alex Tamkin, Karina Nguyen, Brayden McLean, Josiah E. Burke, Tristan Hume, Shan Carter, Tom Henighan, and Christopher Olah. Towards monosemanticity: Decomposing language models with dictionary learning. *Transformer Circuits Thread*, 2023. URL https://transformer-circuits.pub/2023/monosemantic-features.

David Chanin and Adrià Garriga-Alonso. Sparse but Wrong: Incorrect L0 Leads to Incorrect Features in Sparse Autoencoders. *arXiv preprint arXiv:2508.16560*, 2025.

David Chanin, James Wilken-Smith, Tomáš Dulka, Hardik Bhatnagar, and Joseph Bloom. A is for absorption: Studying feature splitting and absorption in sparse autoencoders. *arXiv preprint arXiv:2409.14507*, 2024.

Arpita Chaudhuri, Debasis Samanta, and Monalisa Sarma. Modeling user behaviour in research paper recommendation system. *arXiv preprint arXiv:2107.07831*, 2021.

Runjin Chen, Andy Arditi, Henry Sleight, Owain Evans, and Jack Lindsey. Persona vectors: Monitoring and controlling character traits in language models. *arXiv preprint arXiv:2507.21509*, 2025.

Adam Coates and Andrew Y. Ng. Learning feature representations with K-means. In Grégoire Montavon, Genevieve B. Orr, and Klaus-Robert Müller, editors, *Neural Networks: Tricks of the Trade (2nd edition)*, volume 7700 of *Lecture Notes in Computer Science*, pages 561–580. Springer, 2012.

Jingyi Cui, Qi Zhang, Yifei Wang, and Yisen Wang. On the limits of sparse autoencoders: A theoretical framework and reweighted remedy. In *The Fourteenth International Conference on Learning Representations*, 2026. URL https://openreview.net/forum?id=DSOTgzeH3w.

Hoagy Cunningham, Aidan Ewart, Logan Riggs, Robert Huben, and Lee Sharkey. Sparse autoencoders find highly interpretable features in language models. In *International Conference on Learning Representations (ICLR)*, 2024.

Muhammed Furkan Dasdelen, Hyesu Lim, Michele Buck, Katharina S. Götze, Carsten Marr, and Steffen Schneider. CytoSAE: Interpretable cell embeddings for hematology. *arXiv preprint arXiv:2507.12464*, 2025.

Anders Drachen, Christian Thurau, Rafet Sifa, and Christian Bauckhage. A comparison of methods for player clustering via behavioral telemetry. In *Proceedings of the 8th International Conference on the Foundations of Digital Games (FDG)*, pages 245–252, 2013.

Nelson Elhage, Tristan Hume, Catherine Olsson, Nicholas Schiefer, Tom Henighan, Shauna Kravec, Zac Hatfield-Dodds, Robert Lasenby, Dawn Drain, Carol Chen, Roger B. Grosse, Sam McCandlish, Jared Kaplan, Dario Amodei, Martin Wattenberg, and Christopher Olah. Toy models of superposition. *arXiv preprint arXiv:2209.10652*, 2022.

Dengzhao Fang, Jingtong Gao, Chengcheng Zhu, Yu Li, Xiangyu Zhao, and Yi Chang. HiD-VAE: Interpretable generative recommendation via hierarchical and disentangled semantic IDs, 2025. URL https://arxiv.org/abs/2508.04618.

Leo Gao, Tom Dupré la Tour, Henk Tillman, Gabriel Goh, Rajan Troll, Alec Radford, Ilya Sutskever, Jan Leike, and Jeffrey Wu. Scaling and evaluating sparse autoencoders. *arXiv preprint arXiv:2406.04093*, 2024.

F. Maxwell Harper and Joseph A. Konstan. The MovieLens Datasets: History and Context. *ACM Transactions on Interactive Intelligent Systems (TiiS)*, 5(4):1–19, 2015.

Nick Jiang, Xiaoqing Sun, Lisa Dunlap, Lewis Smith, and Neel Nanda. Interpretable embeddings with sparse autoencoders: A data analysis toolkit, 2025. URL https://arxiv.org/abs/2512.10092.

Hao Kang, Tevin Wang, and Chenyan Xiong. Interpret and control dense retrieval with sparse latent features. In Luis Chiruzzo, Alan Ritter, and Lu Wang, editors, *Proceedings of the 2025 Conference of the Nations of the Americas Chapter of the Association for Computational Linguistics: Human Language Technologies (Volume 2: Short Papers)*, pages 700–709, Albuquerque, New Mexico, April 2025. Association for Computational Linguistics. ISBN 979-8-89176-190-2. doi: 10.18653/v1/2025.naacl-short.58. URL https://aclanthology.org/2025.naacl-short.58/.

Wang-Cheng Kang and Julian McAuley. Self-attentive sequential recommendation. In *2018 IEEE International Conference on Data Mining (ICDM)*, pages 197–206. IEEE, 2018.

Anton Klenitskiy, Konstantin Polev, Daria Denisova, Alexey Vasilev, Dmitry Simakov, and Gleb Gusev. Sparse autoencoders for sequential recommendation models: Interpretation and flexible control. *arXiv preprint arXiv:2507.12202*, 2025.

Anton Korznikov, Andrey Galichin, Alexey Dontsov, Oleg Rogov, Ivan Oseledets, and Elena Tutubalina. Sanity Checks for Sparse Autoencoders: Do SAEs Beat Random Baselines?, 2026. URL https://arxiv.org/abs/2602.14111.

Nhat Minh Le, Ciyue Shen, Neel Patel, Chintan Shah, Darpan Sanghavi, Blake Martin, Alfred Eng, Daniel Shenker, Harshith Padigela, Raymond Biju, Syed Ashar Javed, Jennifer Hipp, John Abel, Harsha Pokkalla, Sean Grullon, and Dinkar Juyal. Learning biologically relevant features in a pathology foundation model using sparse autoencoders. *arXiv preprint arXiv:2407.10785*, 2024.

Yudan Liu, Kaikai Ge, Xu Zhang, and Leyu Lin. Real-time attention based look-alike model for recommender system. In *Proceedings of the 25th ACM SIGKDD International Conference on Knowledge Discovery & Data Mining*, 2019.

Christina Lu, Jack Gallagher, Jonathan Michala, Kyle Fish, and Jack Lindsey. The assistant axis: Situating and stabilizing the default persona of language models. *arXiv preprint arXiv:2601.10387*, 2026.

Jianxin Ma, Chang Zhou, Peng Cui, Hongxia Yang, and Wenwu Zhu. Learning disentangled representations for recommendation. In *Advances in Neural Information Processing Systems (NeurIPS)*, volume 32, 2019.

Subhabrata Mukherjee, Hemank Lamba, and Gerhard Weikum. Item recommendation with evolving user preferences and experience. *arXiv preprint arXiv:1705.02519*, 2017.

Lin Ning, Luyang Liu, Jiaxing Wu, Neo Wu, Devora Berlowitz, Sushant Prakash, Bradley Green, Shawn O'Banion, and Jun Xie. User-LLM: Efficient LLM Contextualization with User Embeddings, 2024. URL https://arxiv.org/abs/2402.13598.

Seongwan Park, Taeklim Kim, and Youngjoong Ko. Decoding dense embeddings: Sparse autoencoders for interpreting and discretizing dense retrieval, 2025. URL https://arxiv.org/abs/2506.00041.

Yang Peng, Changzheng Liu, and Wei Shen. Finding lookalike customers for e-commerce marketing. *arXiv preprint arXiv:2301.03147*, 2023.

Daniel Pluth, Yu Zhou, and Vijay K. Gurbani. Sparse autoencoder insights on voice embeddings. *arXiv preprint arXiv:2502.00127*, 2025.

Senthooran Rajamanoharan, Arthur Conmy, Lewis Smith, Tom Lieberum, Vikrant Varma, János Kramár, Rohin Shah, and Neel Nanda. Improving dictionary learning with gated sparse autoencoders. *arXiv preprint arXiv:2404.16014*, 2024.

Shaina Raza, Mizanur Rahman, Safiullah Kamawal, Armin Toroghi, Ananya Raval, Farshad Navah, and Amirmohammad Kazemeini. A comprehensive review of recommender systems: Transitioning from theory to practice, 2025. URL https://arxiv.org/abs/2407.13699.

Martin Spíšák, Ladislav Peška, Petr Škoda, Vojtěch Vančura, and Rodrigo Alves. From knots to knobs: Towards steerable collaborative filtering using sparse autoencoders. *arXiv preprint arXiv:2601.11182*, 2026.

Fei Sun, Jun Liu, Jian Wu, Changhua Pei, Xiao Lin, Wenwu Ou, and Peng Jiang. BERT4Rec: Sequential Recommendation with Bidirectional Encoder Representations from Transformer. In *Proceedings of the 28th ACM International Conference on Information and Knowledge Management*, pages 1441–1450, 2019.

Adly Templeton, Tom Conerly, Jonathan Marcus, Jack Lindsey, Trenton Bricken, Brian Chen, Adam Pearce, Craig Citro, Emmanuel Ameisen, Andy Jones, Hoagy Cunningham, Nicholas L. Turner, Callum McDougall, Monte MacDiarmid, C. Daniel Freeman, Theodore R. Sumers, Edward Rees, Joshua Batson, Adam Jermyn, Shan Carter, Chris Olah, and Tom Henighan. Scaling monosemanticity: Extracting interpretable features from Claude 3 Sonnet. *Transformer Circuits Thread*, 2024. URL `https://transformer-circuits.pub/2024/scaling-monosemanticity`.

Maolin Wang, Xinjian Zhao, Wanyu Wang, Sheng Zhang, Jiansheng Li, Bowen Yu, Binhao Wang, Shucheng Zhou, Dawei Yin, Qing Li, Ruocheng Guo, and Xiangyu Zhao. Embedding in recommender systems: A survey, 2025. URL `https://arxiv.org/abs/2310.18608`.

Yifan Wang, Suyao Tang, Yuntong Lei, Weiping Song, Sheng Wang, and Ming Zhang. DisenHAN: Disentangled heterogeneous graph attention network for recommendation. In *Proceedings of the 29th ACM International Conference on Information and Knowledge Management (CIKM)*, 2020.

Changshuai Wei, Benjamin Zelditch, Joyce Chen, Andre Assuncao Silva T Ribeiro, Jingyi Kenneth Tay, Borja Ocejo Elizondo, Keerthi Selvaraj, Aman Gupta, and Licurgo Benemann De Almeida. Neural optimization with adaptive heuristics for intelligent marketing system. In *Proceedings of the 30th ACM SIGKDD Conference on Knowledge Discovery and Data Mining*, 2024.

Shitao Xiao, Zheng Liu, Peitian Zhang, and Niklas Muennighoff. C-pack: Packaged resources to advance general Chinese embedding. *arXiv preprint arXiv:2309.07597*, 2023.

Christine Ye, Charles O'Neill, John F Wu, and Kartheik G. Iyer. Steering semantic search with interpretable features from sparse autoencoders. In *MINT: Foundation Model Interventions*, 2024. URL `https://openreview.net/forum?id=oacksuh7Tu`.

Vladimir Zaigrajew, Hubert Baniecki, and Przemysław Biecek. Interpreting CLIP with hierarchical sparse autoencoders. In *Proceedings of the 42nd International Conference on Machine Learning (ICML)*, 2025.

Yu Zheng, Chen Gao, Xiang Li, Xiangnan He, Yong Li, and Depeng Jin. Disentangling user interest and conformity for recommendation with causal embedding. In *Proceedings of the Web Conference 2021 (WWW)*, pages 2980–2991, 2021.

Yongchun Zhu, Yudan Liu, Ruobing Xie, Fuzhen Zhuang, Xiaobo Hao, Kaikai Ge, Xu Zhang, Leyu Lin, and Juan Cao. Learning to expand audience via meta hybrid experts and critics for recommendation and advertising. In *Proceedings of the 27th ACM SIGKDD International Conference on Knowledge Discovery & Data Mining*, 2021.

A Synthetic data experiments

This appendix comprises additional details regarding the synthetic data experiments of Sec. 4.

A.1 Setup

In this experiment, we generate synthetic user–product interactions based on ground truth behavioral modes and test the extent to which various methods can recover them from the embeddings alone. Each ground-truth behavioral mode $\mathcal{P}_k$ is defined by a name, description, product categories, and example products, with an occurrence frequency π_k governing its prevalence. We prompted Claude Opus 4.6 to generate K=75 such modes spanning five domains (Technology & Gaming, Fitness & Outdoors, Home & Kitchen, Lifestyle & Hobbies, Family & Personal Care). The resulting set of behavioral modes is shown in Table 4. With the behavioral modes defined, we generate 100,000 synthetic user shopping histories. For each user $\mathcal{U}$, we sample a number of active behavioral modes $n_{\mathcal{U}} \sim \mathrm{Pois}(\lambda = 2) + 2$, clipped so that $n_{\mathcal{U}} \in [2, 6]$. The specific $n_{\mathcal{U}}$ modes are chosen randomly from the set of all behavioral modes with probability proportional to the popularities π_k, and their weights are drawn independently from $\mathrm{LogNormal}(0, 0.5)$ and normalized to sum to one. We inject noise into the purchase history with weight sampled uniformly from $[0.05, 0.2]$. The total number of orders per user is drawn from a log-normal distribution with underlying-normal parameters $\mu = 4$ and $\sigma = 0.8$ (median $e^4 \approx 55$ interactions), clipped to $[10, 300]$. We allocate the corresponding fraction of interactions to each mode weight plus the noise weight, requiring at least one interaction per active behavioral mode. The generation token budget truncates the longest histories, so realized histories have at most 108 orders (see Appendix A.2).

To generate synthetic user embeddings, we then pass the 100,000 synthetic user profiles described above to Claude Sonnet 4 to generate a corresponding product interaction history for each user. The history generated consists of product names related to each represented behavioral mode. For noise, we provide a list of example product categories and have it inject similar products. Finally, the user embedding is generated by embedding each of the product names in a user's history with a word embedding model, `all-mpnet-base-v2`, and taking their mean. Histories parsed successfully for 99,832 users, with 5,803,030 interactions in total. This results in a 768-dimensional dense embedding for each user that is inherently a superposition of underlying behavioral modes. We L_2-normalize and standardize these embeddings, project them onto random directions in $\mathbb{R}^m$ following [Bingham and Mannila, 2001] to vary the amount of superposition, and then standardize and L_2-normalize the projected embeddings.

A.2 Data statistics

Table 3 and Figure 3 compare item popularity and user activity in the synthetic data with both real datasets. The synthetic data is more head-concentrated than either real dataset, with the top 1% of items carrying 51% of interactions, and its fraction of singleton items lies between theirs. Below the median, synthetic user activity resembles MovieLens, while Open e-commerce has more low-activity users (p50/p10 activity ratio 2.89, vs. 3.56 for MovieLens and 6.63 for Open e-commerce). Above the median, the generation budget truncates the synthetic upper tail near twice the median. The synthetic data therefore reproduces the short head and long tail of item popularity that characterize real-world user interaction data. This implies the recovery results of Section 4 do not depend on unrealistically uniform item popularity. The synthetic data distribution differs from the real-world examples considered primarily by lacking very heavy users.

Table 3: Item popularity in the synthetic data and both real datasets: share of interactions carried by the most popular 1% and 10% of items, and the fraction of items that appear exactly once.

Dataset	Items	Interactions per item	Top 1%	Top 10%	Singletons
Synthetic	778,639	7.5	50.9%	79.7%	62.3%
Open e-commerce (ASIN)	939,082	2.0	19.1%	45.8%	75.6%
MovieLens 1M	3,706	270	8.7%	44.4%	3.1%

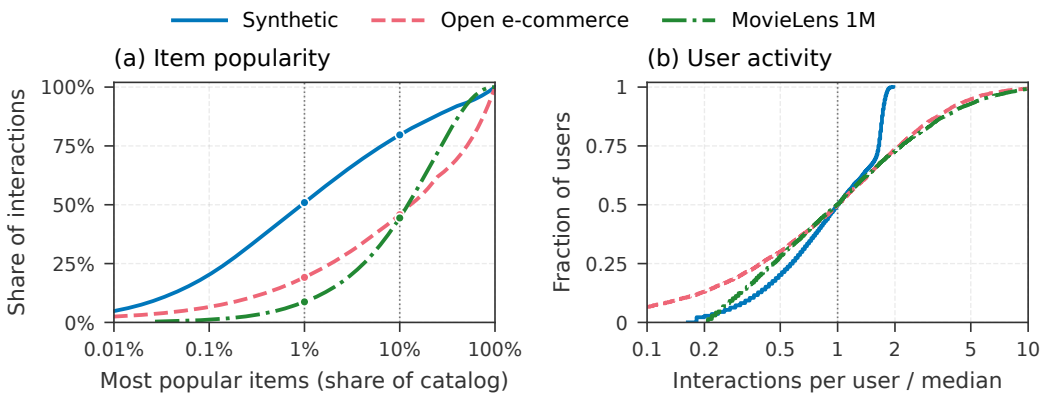


Figure 3: Item popularity and user activity for the synthetic data and both real datasets. (a) Share of interactions carried by the most popular items, with dots at the top 1% and 10% of items (cf. Table 3). (b) Interactions per user divided by each dataset's median. Synthetic histories are bounded at about 100 interactions by the generation budget, which truncates the upper tail.

A.3 SAE and other baselines

For the SAE, we take the vanilla ReLU version described in Eq. (3), with an adaptive λ sparsity penalty to match the ground truth L_0. Here, λ is warmed up for 10 epochs, then $\log \lambda$ is adjusted each epoch by an amount proportional to the difference between current and target L_0. The SAE has $d_{\text{hidden}} = 300$ and is trained for 50 epochs with batch size 256 and learning rate 10^{-3}.

We consider six additional baselines: random projections onto 300 unit vectors (the SAE's width) with ReLU, sparsified versions of PCA and FastICA, K-Means encoding (cosine similarity to K-Means centroids passed through ReLU and thresholded to match the ground-truth L_0, following [Coates and Ng, 2012]), the soft-frozen decoder SAE of [Korznikov et al., 2026], and NMF on shifted (non-negative) embeddings. K-Means encoding uses 75 components matching the ground-truth mode count, and PCA, ICA, and NMF use $\min(75, m)$. The soft-frozen decoder uses identical hyperparameters to the SAE. To ensure fair comparison, we sparsify all non-SAE methods except NMF to match the ground-truth mean L_0 by zeroing activations below a calibrated threshold. NMF retains its natural sparsity, as we find additional thresholding degrades its performance. Note that every time we report results on these methods, they correspond to the sparsified versions.

A.4 Mode recovery at other cosine thresholds

The conclusions of Figure 1 do not hinge on the 0.7 cosine cutoff for mode recovery. Repeating the evaluation at thresholds from 0.5 to 0.8, the SAE recovers more modes than FastICA, PCA, and NMF at every threshold and every m, and more than every classical baseline in Figure 1 for $m \geq 32$. At $m \leq 24$, K-Means encoding matches the SAE at 0.7 ($m = 16$) and exceeds it at 0.8, but its recovery does not improve with dimension (0.69 to 0.74 at 0.8 across all m), whereas the SAE's rises from 0.47 at $m = 16$ to 0.98 at $m = 128$ and overtakes it from $m = 32$. K-Means centroids thus capture a fixed fraction of the modes regardless of how much room the embedding leaves to separate them, while the SAE uses the additional dimensions.

A.5 Soft-frozen-decoder baseline

Korznikov et al. [2026] point out that SAEs can fail to learn the underlying features from LLM activations, with performance matched or exceeded by simple random baselines in high-dimensional regimes. To check whether this equivalence holds in our setup, we train a soft-frozen-decoder variant alongside the standard SAE [Korznikov et al., 2026]. The soft-frozen variant uses identical hyperparameters to the fully trained SAE (adaptive L_1 to match ground-truth average L_0, same learning rate and starting λ), so any divergence between the two isolates the contribution of decoder training.

Table 4: Complete taxonomy of the 75 synthetic behavioral modes used as ground truth for the synthetic experiments of Section 4. Each behavioral mode was generated with a name, description, product categories, and example products (not shown for compactness); only the name and domain grouping are displayed here.

ID	Behavioral mode	Domain
Technology & Gaming		
1	Tech Enthusiast	Tech/Electronics
2	Mobile Gamer	Gaming
3	PC Gamer	Gaming/Hardware
4	Smart Home Builder	IoT/Automation
5	Audiophile	Audio
6	Console Collector	Gaming/Collectibles
7	Photography Hobbyist	Cameras/Lenses
8	Drone Pilot	Drones/Outdoor
9	VR Enthusiast	VR/Gaming
10	Streaming Creator	Audio/Video
11	3D Printing Maker	Manufacturing
12	Mechanical Keyboard Builder	Keyboards/DIY
13	Home Theater Buff	Audio/Video
14	Tablet Power User	Tablets/Productivity
15	Network Admin Hobbyist	Networking
Fitness & Outdoors		
16	Gym Regular	Fitness/Nutrition
17	Marathon Runner	Running/Training
18	Yoga Practitioner	Yoga/Wellness
19	Cycling Enthusiast	Cycling/Outdoor
20	Hiking Adventurer	Hiking/Camping
21	Rock Climber	Climbing/Safety
22	Camping Enthusiast	Camping/Survival
23	Swimmer	Swimming/Fitness
24	CrossFit Athlete	CrossFit/Training
25	Skier/Snowboarder	Winter Sports
26	Tennis Player	Tennis/Sports
27	Golfer	Golf/Sports
28	Kayaker	Water Sports
29	Home Gym Builder	Home Fitness
30	Martial Artist	Martial Arts
Home & Kitchen		
31	Home Chef	Cookware/Kitchen
32	Baking Enthusiast	Baking/Tools
33	Coffee Connoisseur	Coffee/Beverages
34	Meal Prepper	Meal Prep/Storage
35	Grilling Master	Grilling/BBQ
36	Wine Enthusiast	Wine/Accessories
37	Home Bartender	Bar/Cocktails
38	Tea Lover	Tea/Beverages
39	Fermentation Hobbyist	Fermentation/DIY
40	Instant Pot User	Appliances
41	Air Fryer Fan	Appliances/Health
42	Sous Vide Cook	Precision Cooking
43	Indoor Gardener	Hydroponics/Plants
44	Kitchen Gadget Collector	Gadgets/Tools
45	Minimalist Chef	Quality Essentials

A.6 Transformer embeddings of the synthetic data

To test recovery when the embedding is produced by a trained sequence encoder, we train SASRec with the MovieLens configuration of Appendix E.1 (d_{model}=256, 4 heads, 2 layers, `max_len`=200, dropout 0.3, learning rate 5×10^{-4}) on the synthetic interaction sequences. Items are normalized product names that appear at least 5 times (119,826 items covering 83.9% of interactions, 99,213 users), and each user's history is shuffled, since the generative model draws interactions independently. The encoder reaches a test HR@10 of 0.93. User embeddings are the mean of final-layer hidden

Table 5: Complete taxonomy of the 75 synthetic behavioral modes used as ground truth (continued).

ID	Behavioral mode	Domain
Lifestyle & Hobbies		
46	Book Lover	Books/Literature
47	Board Game Enthusiast	Gaming/Tabletop
48	Puzzle Solver	Puzzles/Games
49	Craft Enthusiast	Crafts/DIY
50	Knitter/Crocheter	Yarn/Crafts
51	Painting Artist	Art Supplies
52	Model Builder	Model Kits
53	Gardening Hobbyist	Gardening/Outdoor
54	Aquarium Keeper	Aquarium/Fish
55	Vinyl Collector	Music/Audio
56	Journaling Enthusiast	Stationery/Writing
57	Candle Maker	Candle Making/DIY
58	Birdwatcher	Birdwatching/Nature
59	Astronomy Hobbyist	Astronomy/Optics
60	Miniature Painter	Miniatures/Gaming
Family & Personal Care		
61	New Parent	Baby/Childcare
62	Pet Parent – Dog	Pet Supplies
63	Pet Parent – Cat	Pet Supplies
64	Skincare Enthusiast	Skincare/Beauty
65	Makeup Enthusiast	Cosmetics/Beauty
66	Hair Care Devotee	Hair Care/Styling
67	Fragrance Collector	Perfume/Luxury
68	Natural Beauty Advocate	Organic/Eco-Friendly
69	Nail Art Enthusiast	Nail Care/Beauty
70	Wellness Seeker	Wellness/Health
71	Dental Care Focused	Dental/Health
72	Men's Grooming	Grooming/Skincare
73	Jewelry Lover	Jewelry/Fashion
74	Fashion Shopper	Clothing/Accessories
75	Minimalist Wardrobe	Quality Basics

states, standardized and L_2-normalized, and the SAE (d_{hidden}=300) and baselines are run exactly as in Section 4. Items are not mode-exclusive: 15 to 20% of interaction mass falls on noise items bought across modes, and the mass-weighted mode purity over all items is 0.74 (1.0 would be perfectly exclusive).

Table 6 reports recovery at d=256. A linear readout still recovers most of the mode information (oracle 0.78, vs. 0.85 for the mean-pooled product embeddings at m=256), so the encoder preserves the modes, and the SAE recovers them best. It leads on code–GT alignment and recovers 73 of 75 modes at cosine ≥ 0.7 (97 to 100% across repeated SAE trainings on the same embeddings), while the classical baselines lose much more relative to the mean-pooled case, FastICA falling from 95% to 59% recovery. FastICA keeps the highest per-feature correlation, as in Section 4, and merging raises the SAE's from 0.28 to 0.54. Per-mode recovery correlates with the fraction of a mode's interactions that survives the vocabulary threshold (Spearman $\rho = 0.31$). LDA, fit to the raw user–item counts with 75 topics and sparsified to the same L_0, recovers real structure but trails the SAE on both metrics it supports, consistent with the claim in Section 2 that embeddings carry more recoverable mode structure than raw counts. Doubling its training iterations changes its alignment by less than 0.01.

The same picture holds under further compression and when the encoder itself must superpose the modes. Randomly projecting the d=256 embeddings to $m = 16$ to 128 (5 projections each), the SAE recovers more modes than PCA, FastICA, and K-Means encoding at every m, although FastICA attains higher alignment for $m \geq 48$. An encoder trained at d_{model}=64 $< K$ has a lower ceiling (oracle 0.58), yet the SAE still has the best alignment (0.41, vs. 0.36 for FastICA) and recovers 97% of modes at cosine ≥ 0.5 and 71% at ≥ 0.7, while FastICA recovers none at either threshold. Finally, Table 7 varies the number of modes. Restricting the population to users whose active modes all lie among the K' most popular modes gives exact K'-mode ground truth, and the SAE (with $d_{\text{hidden}} = 4K'$) captures a nearly constant 73 to 75% of the oracle ceiling while matching or exceeding

Table 6: Mode recovery on mean-pooled SASRec embeddings (d=256) of the synthetic data, all methods at matched L_0. LDA is fit to raw user–item counts and has no decoder directions.

Method	Code–GT alignment	Median per-feature r	Modes recovered (cos ≥ 0.7)
Oracle (linear ceiling)	0.78	—	—
SAE	**0.58**	0.28	**0.97**
SAE (merged)	0.54	0.54	0.95
FastICA	0.53	**0.62**	0.59
K-Means encoding	0.45	0.30	0.52
PCA	0.25	0.17	0.00
LDA (raw counts)	0.37	0.27	—

the best classical baseline at every K'. The restriction selects users with fewer and more concentrated modes, which is why we report the oracle-normalized ratio, and $K' = 10$ leaves too few users (2,043) to evaluate.

Table 7: Sensitivity to the number of modes K' on the d=256 transformer embeddings. Code–GT alignment for the oracle, the SAE, and the best of PCA, FastICA, and K-Means encoding at each K'.

K'	Users	Oracle	SAE	Best classical	SAE / oracle
15	4,591	0.943	0.695	0.667	0.737
20	8,394	0.931	0.683	0.598	0.734
25	13,245	0.918	0.679	0.643	0.740
30	19,880	0.897	0.651	0.631	0.725
40	36,737	0.871	0.642	0.623	0.737
50	58,248	0.838	0.619	0.617	0.739
60	79,007	0.809	0.604	0.572	0.747
75	99,213	0.779	0.581	0.526	0.746

B Additional baselines: PCA, ICA

The main text reports SAE (primary) and K-Means encoding on both datasets, plus FastICA on Open e-commerce (its closest classical competitor). For completeness, Table 8 reports PCA and FastICA on both datasets at matched mean L_0. PCA and ICA are capped at the input dimension by construction (d=128 on Open e-commerce, d=256 on MovieLens), since orthogonal/independent components cannot be overcomplete. SAE and K-Means encoding use the SAE's dictionary width (d_{hidden}=512 for Open e-commerce, d_{hidden}=1024 for MovieLens). Numbers are averaged across tasks within each dataset.

Table 8: Additional baselines on both datasets. Metrics averaged across tasks. SAE significantly exceeds every classical baseline on Lift at matched L_0 (cross-seed Wilcoxon, Appendix D); ICA is SAE's closest competitor on AUROC (tied on life-event AUROC, SAE wins elsewhere) and achieves higher Coverage by construction (denser activations). NMF is excluded as it requires non-negative preprocessing that doesn't naturally arise in either embedding space and underperforms classical baselines at all m (Section 4).

Dataset	Method	FVU ↓	Lift	AUROC	Coverage
Open e-commerce	PCA	0.388	1.28×	0.579	0.797
	ICA	0.083	1.86×	0.695	0.770
MovieLens (SASRec)	PCA	0.189	1.65	0.576	0.815
	ICA	0.343	1.99	0.610	0.910
MovieLens (BERT4Rec)	PCA	0.200	1.60	0.592	0.904
	ICA	0.357	2.08	0.580	0.833

C Open e-commerce additional details

C.1 Embedding generation

Embeddings are generated by segmenting user order histories into 6-month chunks, constructing the user-category count matrix on each chunk (1864 categories with > 5 purchases in any window),

applying log scaling and TF-IDF weighting, L_2-normalizing each row, and taking truncated SVD with embedding dimension 128. The SAE is trained directly on these embeddings. No text input enters the decomposition pipeline at any point. We select the SAE operating point following the decoder-orthogonality criterion of [Chanin and Garriga-Alonso, 2025], giving d_{hidden}=512 (4× overcomplete), λ=5×10^{-4}, 25 epochs, and mean L_0≈23. All 512 latents remain live after training (no dead features). We use Claude Sonnet 4.6 to auto-interpret each latent, passing 10 high-activating positives and 10 random negatives and asking the model to identify the behavioral pattern present in the positives and absent in the negatives, producing a short feature name (e.g., "Premium_Dog_Food_Buyers") and one-sentence description. Full prompts are in Appendix F. Reported retrieval numbers are averaged over 5 SAE training seeds with the same operating point, and cross-seed paired Wilcoxon tests are reported in Appendix D.

C.2 Tasks and ground truth

We consider 6 *category retrieval* tasks spanning base rates 8–54% (pet owner, coffee enthusiast, gardener, board gamer, baby products, musician), and 2 *life-event retrieval* tasks from the companion survey (new parent in 2021, moved residence in 2021). Other survey life events (e.g., divorced, changed jobs) either had insufficient positive counts or did not correlate with category-level behavior changes, and are excluded. Early in experimentation we considered two additional category tasks (Fisher, Photographer) for which the retrieval pipeline's default gating settings did not allow any features through for at least one method; per-method retuning would eliminate the zero-return behavior, but we instead fix the operating point across methods for apples-to-apples comparison of feature and interpretation quality. For category tasks, positives are users who purchased in the target categories in post-2021 windows; we use the dataset's canonical category definitions for each task (listed in Table 9). For life-event tasks, positives are users who self-reported the event in 2021.

Table 9: Open e-commerce task definitions. n_{pos} is the number of users satisfying the positive definition out of the evaluated user set for each task block (4085 users with at least one post-2021 window for category retrieval; 4373 users with a 2021 survey response for life-event retrieval).

Task type	Task name	n_{pos}	Base rate
Category retrieval	Musician	345	8.4%
	Baby products	839	20.5%
	Board gamer	1421	34.8%
	Coffee enthusiast	1482	36.3%
	Gardener	1539	37.7%
	Pet owner	2196	53.8%
Life-event retrieval	New parent (2021)	226	5.2%
	Moved residence (2021)	942	21.5%

C.3 Retrieval strategies

SAE + NL (main-text primary) presents all feature interpretations to an LLM alongside a natural-language audience query, which scores each feature's relevance on a 0–10 scale; we retain features scoring ≥ 5 and rank users by the weighted sum of their activations on the retained features. This strategy is fully zero-shot: it sees only the NL query and the feature interpretations.

K-Means encoding + NL uses the same scoring and ranking pipeline, substituting K-Means-encoding features for SAE features.

Text-embedding baseline requires no sparse decomposition. For each user we embed the NL query with `all-MiniLM-L6-v2` and rank users by cosine similarity to a per-user text vector. The user vector is the *category-pooled* variant: a TF-IDF-weighted mean of sentence-transformer embeddings over the user's purchased category names (with underscores replaced by spaces and lowercased so the encoder receives natural-language phrases). This is the matched-input fair comparison: the SAE, K-Means encoding, and ICA consume exactly the same TF-IDF-weighted category signal, so any retrieval advantage over this baseline is attributable to the decomposition itself rather than to extra text the baseline did not see.

Raw category counts ranks users by their pre-2021 purchase counts in each task's target categories. It is an oracle for the category-retrieval block (it uses the ground-truth category definition) and a

category-based approximation for the life-event block (using hand-picked proxy categories such as diapers/baby food for "new parent"). We include it as a ceiling, not as a comparison target.

SAE + correlation (reported here for completeness only; not zero-shot) selects the 20 SAE features most correlated with target-category purchases in pre-2021 data, then ranks users by their weighted activations on those features. This requires access to the target category list for each task and is therefore not a zero-shot method. We report its numbers as a reference point for how much signal the SAE features carry when supervised feature selection is applied.

C.4 Task-type breakdown

Category-retrieval tasks. Aggregate 5-seed means are in Table 1; cross-seed p-values are in Table 10. A supervised *SAE+correlation* variant selects the 20 SAE features most correlated with per-task target-category purchases in pre-2021 data and ranks users by weighted activation on those features. This variant is not zero-shot and requires the per-task category list that SAE+NL does not see. At matched L_0 it reaches mean Lift@n_{pos} of $\approx 1.9\times$ and mean AUROC of ≈ 0.72, roughly matching the zero-shot SAE+NL variant on both. The SAE dictionary therefore contains enough per-task signal to recover supervised-ranking quality from unsupervised decomposition alone.

Life-event tasks. The category-counts column here is a keyword-proxy, not an oracle: past purchases of hand-picked proxy categories (diapers, baby food) do not pre-identify users who will *become* parents, and no comparable proxy list exists for residential mobility. SAE+NL beats K-Means encoding and PCA on Lift, AUROC, and $\text{AUROC}_{\text{scored}}$ with cross-seed $p{=}0.001$ (10 paired seed–task observations; Table 10). Against ICA, SAE wins Lift and $\text{AUROC}_{\text{scored}}$ ($p{=}0.001$–0.002) and ties on AUROC ($p{=}0.5$, 0.715 vs. 0.713). ICA achieves higher Coverage than SAE on both tasks due to its denser activations, mirroring the category-task pattern.

C.5 Open-weight interpretation model

We chose Claude Sonnet 4.6 for interpretation because it was among the strongest models at its scale and was available for large-scale batch inference on our platform. To test whether the retrieval results depend on the interpretation model, we re-name the features of one Open e-commerce seed with the open-weight Llama 3.3 70B Instruct (via Amazon Bedrock, temperature 0), holding everything else fixed: the same SAE and baseline codes, the same sampled users and prompts, and the same Claude Haiku 4.5 query-time scoring. Llama's names closely track Sonnet's. The median sentence-embedding cosine between the two models' name-and-description strings for the same feature is 0.64 to 0.69 across methods, against 0.29 to 0.35 for different features. Llama assigns nearly constant confidence scores (0.92 ± 0.01), so the 0.6 confidence filter passes every feature, and we therefore also evaluate Llama's names paired with Sonnet's confidence scores. In both variants the SAE remains ahead of every baseline on mean Lift in both task blocks, and its own Lift stays within 6% of the Sonnet-named value on at least 6 of the 8 tasks. Its margins over FastICA and K-Means encoding narrow, however. With Llama's names, the SAE's category-task AUROC lead over K-Means encoding falls from 0.031 to under 0.01, and its life-event Lift lead over FastICA from 0.32 to about 0.03. For scale, re-running query-time scoring on the Sonnet names alone changes Lift by up to 0.012 on category tasks and 0.09 on life-event tasks, since the scoring is not fully deterministic. The direction of the comparison therefore does not depend on the interpretation model, but its size partly does. Llama's names lead the query-time gate to admit more features per query for every method (21 vs. 14 for the SAE), which raises the baselines' coverage (K-Means encoding on category tasks, 0.61 to 0.75) while the SAE's barely changes. Part of the SAE's margin under Sonnet thus comes from how features are named and selected rather than from the decomposition alone. This replication uses a single seed and no significance test.

D Statistical significance tables

Table 10 consolidates all Wilcoxon signed-rank tests and Stouffer combinations referenced in the main text. All tests are one-sided with alternative hypothesis SAE $>$ baseline. The direction is pre-specified by the hypothesis, not chosen after observing the data. For tests where the baseline wins we report the reverse-direction p-value rather than suppressing the comparison.

Open e-commerce tests are paired across 5 seeds $\times$ task (6 category tasks or 2 life-event tasks) as cross-seed paired observations. MovieLens retrieval tests are paired across the 32 non-compositional NL audience queries, reported separately per encoder and Stouffer-combined. Audience-characterization tests are paired across 20 franchise audiences, Stouffer-combined across the two MovieLens encoders.

Table 10: Consolidated paired Wilcoxon one-sided p-values. Default alternative H1: SAE > baseline on the named metric. Bold indicates $p<0.05$ *in the SAE-wins direction*; reverse-direction losses are reported unbolded for clarity. MovieLens retrieval columns report per-encoder and Stouffer-combined p; Open e-commerce and audience-characterization sections are single-dataset (e-commerce) or Stouffer-combined across MovieLens encoders (audience). Stouffer across encoders assumes independence; here the two encoders share users and queries, so combined p-values should be read as descriptive summaries rather than independence-based combinations (per-encoder columns are the primary quantity). **Note on pairing:** Open e-commerce and MovieLens SAE-vs-K-Means rows are cross-seed (Open e-commerce: 5 seeds × task; MovieLens: 2 SAE-training seeds × 32 queries). MovieLens rows vs. PCA/ICA/text are single-seed paired across 32 queries. †For top-5 redundancy (median pairwise cosine among the top-5 features), smaller is more diverse; alternative hypothesis is H1: K-Means redundancy > SAE redundancy. ‡For tests where the named comparison wins in the reverse direction, the reported p is the reverse-direction one-sided value (equal to $1 - p_{\text{primary}}$) rather than the alternative-hypothesis p .

	Comparison	One-sided p
Open e-commerce category retrieval (cross-seed paired Wilcoxon, 5 seeds × 6 tasks)		
Lift@n_{pos}	SAE vs K-Means encoding	$\mathbf{p = 0.0003}$
Lift@n_{pos}	SAE vs ICA	$\mathbf{p = 0.0002}$
Lift@n_{pos}	SAE vs PCA	$\mathbf{p < 10^{-4}}$
AUROC	SAE vs K-Means encoding	$\mathbf{p < 10^{-4}}$
AUROC	SAE vs ICA	$\mathbf{p = 0.004}$
AUROC	SAE vs PCA	$\mathbf{p < 10^{-4}}$
$\text{AUROC}_{\text{scored}}$	SAE vs K-Means encoding	$\mathbf{p = 0.009}$
$\text{AUROC}_{\text{scored}}$	SAE vs ICA	$\mathbf{p = 0.0003}$
$\text{AUROC}_{\text{scored}}$	SAE vs PCA	$\mathbf{p < 10^{-4}}$
Coverage	SAE vs K-Means encoding	$\mathbf{p < 10^{-4}}$
Coverage	SAE vs ICA‡	$p = 0.91$ (ICA wins)
Coverage	SAE vs PCA‡	$p = 1.0$ (PCA wins)
Open e-commerce life-event retrieval (cross-seed paired Wilcoxon, 5 seeds × 2 tasks)		
Lift@n_{pos}	SAE vs K-Means / ICA / PCA	$\mathbf{p = 0.001}$ (each)
AUROC	SAE vs K-Means / PCA	$\mathbf{p = 0.001}$ (each)
AUROC	SAE vs ICA	$p = 0.50$ (tied, 0.715 vs 0.713)
$\text{AUROC}_{\text{scored}}$	SAE vs K-Means / ICA / PCA	$\mathbf{p \leq 0.002}$ (each)
Coverage	SAE vs K-Means	$\mathbf{p = 0.007}$
Coverage	SAE vs ICA‡	$p = 0.97$ (ICA wins)

MovieLens NL audience retrieval (n=32 queries)

		SASRec	BERT4Rec	Stouffer
Lift@n_{pos}	SAE vs K-Means encoding	0.36	0.69	0.54
Lift@n_{pos}	SAE vs PCA	**0.0003**	**0.0008**	$< 10^{-4}$
Lift@n_{pos}	SAE vs ICA	**0.0012**	**0.0014**	$< 10^{-4}$
Lift@n_{pos}	SAE vs text baseline	**0.0070**	**0.0028**	**0.0001**
AUROC	SAE vs K-Means encoding	0.100	0.81	0.41
AUROC	SAE vs PCA	$< 10^{-4}$	$< 10^{-4}$	$< 10^{-4}$
AUROC	SAE vs ICA	$< 10^{-4}$	$< 10^{-4}$	$< 10^{-4}$
AUROC	SAE vs text baseline	0.895	0.661	0.881
$\text{AUROC}_{\text{scored}}$	SAE vs K-Means encoding	**0.014**	0.07	**0.005**
$\text{AUROC}_{\text{scored}}$	SAE vs PCA	$< 10^{-4}$	**0.0001**	$< 10^{-4}$
$\text{AUROC}_{\text{scored}}$	SAE vs ICA	$< 10^{-4}$	$< 10^{-4}$	$< 10^{-4}$
$\text{AUROC}_{\text{scored}}$	SAE vs text baseline	0.943	0.688	0.928
Coverage	SAE vs K-Means encoding	$< 10^{-4}$	$< 10^{-4}$	$< 10^{-4}$
Coverage	SAE vs PCA	**0.0002**	**0.0036**	$< 10^{-4}$
Coverage	SAE vs ICA	**0.017**	$< 10^{-4}$	$< 10^{-4}$
Coverage	SAE vs text baseline	1.000	1.000	1.000
Audience characterization (n=20 franchises, Stouffer across encoders)				
Slate redundancy (K-Means>SAE)†	median pairwise cosine	**0.002**	**0.049**	$\approx 4\times10^{-4}$
Reverse-selector coverage	SAE vs K-Means encoding	**0.0003**	**0.0001**	$\approx 10^{-7}$

E MovieLens additional details

E.1 Width-and-sparsity sweep

Transformer recommenders. SASRec [Kang and McAuley, 2018] and BERT4Rec [Sun et al., 2019] both use d_{model}=256, 4 heads, 2 layers, `max_len`=200, dropout 0.3, learning rate 5×10^{-4}, trained on chronologically ordered interactions. User embeddings are the mean of non-padding final-layer hidden states.

SAE operating point. We selected the SAE operating point reported in Section 5.2 using the decoder-orthogonality criterion of [Chanin and Garriga-Alonso, 2025]: we sweep λ at a fixed width and pick the elbow of mean pairwise decoder cosine similarity (c_{dec}). Among widths satisfying this elbow condition, we choose the smallest width that maintains a high absolute count of features with sufficient statistical support for reliable auto-interpretation (30–500 activating users, "eligible" in what follows). Our final choice is d_{hidden}=1024 with λ=1.98×10^{-3}. The same λ is used for both encoders. Measured L_0 differs only slightly ($\approx$80 on SASRec, $\approx$83 on BERT4Rec), giving a direct architecture-level comparison at a matched sparsity target.

Width and sparsity. Table 11 reports representative rows of the sweep on SASRec embeddings at d_{hidden}=1024. c_{dec} flattens for $L_0 \in [65, 100]$, indicating an elbow beyond which additional sparsity pressure does not further improve decoder orthogonality. Within this band, $L_0\approx80$ maximizes eligible feature count. The same qualitative picture holds for BERT4Rec embeddings. Widths below 1024 ($d\in\{256, 512\}$) cap eligible-feature yield at under 30% and were ruled out; d=2048 exhibited high dead-feature counts without improving either metric.

Table 11: Width-and-sparsity sweep on MovieLens SASRec embeddings at d_{hidden}=1024. Selected operating point (bold) sits at the c_{dec} elbow with the highest eligible-feature count. "Eligible" counts features with 30–500 activating users.

λ	mean L_0	c_{dec}	% eligible	n eligible	recon. MSE
5.70×10^{-3}	68.7	0.095	24.5%	251	0.060
3.62×10^{-3}	65.9	0.080	24.6%	252	0.044
1.98×10^{-3}	**82.8**	**0.081**	**37.1%**	**380**	**0.026**
1.46×10^{-3}	102.3	0.083	43.6%	446	0.021
8.30×10^{-4}	147.7	0.086	38.0%	389	0.014

Decoder-cosine distributions. Pairwise decoder cosines are centered near zero for the SAE on both encoders (mean 0.0001 on SASRec, 0.0008 on BERT4Rec), confirming the near-orthogonal geometry claimed in Section 5.2. K-Means encoding's centroids are natively denser (mean pairwise cosine 0.29 on SASRec, 0.17 on BERT4Rec).

Training length. Table 12 reports a training-length sensitivity check at the selected (d, λ) configuration. Training past 250 epochs begins to over-sparsify the dictionary: eligible-feature count declines as features slip below the 30-user support threshold, and c_{dec} worsens because the dying features leave behind overlapping decoder directions. Shorter training (125 epochs) produces a higher raw eligible count, but inspection of the top features reveals within-theme redundancy (e.g. multiple distinct "classic Western" latents) that an overcomplete dictionary has not yet deduplicated. We therefore train to 250 epochs for both encoders, which sits at the inflection point between under- and over-training.

E.2 Natural-language audience queries and ground truth

Table 13 lists the 32 non-compositional natural-language audience queries used in the MovieLens retrieval evaluation, along with the title patterns and optional MovieLens-genre constraint used to resolve each query to a ground-truth positive set. Ground-truth labels are generated by a deterministic rule: for query Q with title-pattern set $\mathcal{P}_Q$ and optional genre constraint $\mathcal{G}_Q$, a user is labelled positive if their MovieLens watch history contains ≥ 3 movies whose title matches any pattern in $\mathcal{P}_Q$ (case-insensitive substring match) *and* whose MovieLens-listed genres include every genre in $\mathcal{G}_Q$. Queries yielding fewer than 20 positive users in the evaluated population are dropped from

Table 12: Training-length sensitivity at d_{hidden}=1024, λ=1.98×10^{-3} on SASRec embeddings. Selected training length (bold) balances feature count against within-theme redundancy. Metrics at 250 epochs differ slightly from the corresponding row in Table 11 because the two tables report independent training runs; seed-level variation on MovieLens SAE training can reach $\sim$10% on L0 and reconstruction MSE at a fixed operating point (see seed-variance discussion in the supplementary notes).

Epochs	mean L_0	c_{dec}	n eligible	n too-rare	recon. MSE
125	101.0	0.054	653	0	0.091
250	**80.2**	**0.059**	**572**	**125**	**0.052**
500	74.3	0.076	498	165	0.033

the benchmark. One such dropped query, *"viewers who enjoy martial arts and kung fu films"*, falls below the floor on MovieLens 1M and is excluded. The remaining 32 are retained. Queries split into 21 broad audiences (e.g. Tarantino fans, Disney animation) and 11 niche audiences (e.g. French New Wave, pre-1960 film noir). Draft query strings and candidate title-pattern lists were generated with Claude Opus 4.6 and then curated by the authors against the MovieLens 1M catalog. The final patterns used to produce ground-truth labels are those listed in Table 13. Paired Wilcoxon p-values for per-query SAE-vs-baseline comparisons are consolidated in Appendix D, Table 10.

The text-embedding baseline evaluated alongside SAE and K-Means encoding scores each user by the cosine similarity between the query embedding and the user's mean-pooled watched-title embedding (both computed with `all-MiniLM-L6-v2`).

Table 13: Natural-language audience queries on MovieLens 1M with title-pattern and genre-constraint ground-truth definitions. n_+ is the resulting number of positive users out of 6040.

Query	Title patterns (representative)	Genre	n_+
Broad audiences (21 queries)			
Fans of Quentin Tarantino films	Pulp Fiction, Reservoir Dogs, Jackie Brown, Kill Bill, Four Rooms	—	517
Fans of Steven Spielberg adventure and sci-fi films	Raiders of the Lost Ark, Indiana Jones, Jurassic Park, E.T., Close Encounters, . . . (9 total)	—	3099
Fans of classic Disney animated films	Lion King, Little Mermaid, Beauty and the Beast, Aladdin, Snow White, . . . (21 total)	—	1682
Viewers of dark, psychological thrillers	Silence of the Lambs, Se7en, Fight Club, American Psycho, Memento, . . . (13 total)	—	1748
Fans of romantic comedies from the 1990s	Pretty Woman, Sleepless in Seattle, You've Got Mail, Notting Hill, Four Weddings, . . . (10 total)	Romance/ Comedy	1237
Fans of Stanley Kubrick films	Clockwork Orange, 2001: A Space Odyssey, Shining, Full Metal Jacket, Dr. Strangelove, . . . (10 total)	—	1385
Fans of Star Wars and space opera	Star Wars, Empire Strikes Back, Return of the Jedi, Phantom Menace	—	2237
Viewers who enjoy classic film noir and crime dramas	Chinatown, Maltese Falcon, Double Indemnity, Third Man, Sunset Blvd, . . . (10 total)	—	1019
Fans of Monty Python and British comedy	Monty Python and the Holy Grail, Life of Brian, Meaning of Life, Fish Called Wanda, Time Bandits	—	758
Viewers who enjoy horror and slasher films	Nightmare on Elm Street, Halloween, Friday the 13th, Texas Chain Saw, Scream, . . . (14 total)	Horror	1078
Fans of epic historical war films	Saving Private Ryan, Braveheart, Gladiator, Schindler's List, Platoon, . . . (11 total)	War	2228

Continued on next page.

Table 13 (continued)

Query	Title patterns (representative)	Genre	n_+
Fans of quirky independent and arthouse films	Fargo, Big Lebowski, Raising Arizona, Barton Fink, Being John Malkovich, . . . (13 total)	—	4504
Fans of slapstick and physical comedy	Airplane!, Naked Gun, Blazing Saddles, Young Frankenstein, Ace Ventura, . . . (11 total)	—	1887
Fans of Tim Burton's gothic and fantasy films	Edward Scissorhands, Beetlejuice, Batman, Batman Returns, Nightmare Before Christmas, . . . (8 total)	—	1591
Viewers who enjoy coming-of-age teen dramas	Breakfast Club, Sixteen Candles, Ferris Bueller, Stand By Me, Dead Poets Society, . . . (10 total)	—	1545
Fans of classic musicals	Singin' in the Rain, Sound of Music, West Side Story, Wizard of Oz, My Fair Lady, . . . (10 total)	Musical	1055
Viewers interested in courtroom and legal dramas	12 Angry Men, Few Good Men, To Kill a Mockingbird, Verdict, Primal Fear, . . . (10 total)	—	930
Fans of Woody Allen films	Annie Hall, Manhattan, Hannah and Her Sisters, Crimes and Misdemeanors, Sleeper, . . . (13 total)	—	935
Fans of the Coen Brothers films	Fargo, Big Lebowski, Raising Arizona, Barton Fink, Miller's Crossing, . . . (9 total)	—	873
Fans of Martin Scorsese films	Taxi Driver, Raging Bull, GoodFellas, Casino, Mean Streets, . . . (12 total)	—	945
Fans of Alfred Hitchcock films	Psycho, Vertigo, Rear Window, North by Northwest, Birds, . . . (17 total)	—	1301
Niche audiences (11 queries)			
Viewers who enjoy Studio Ghibli and Japanese animation	Princess Mononoke, My Neighbor Totoro, Kiki's Delivery Service, Nausicaä, Castle in the Sky, . . . (8 total)	—	97
Viewers who enjoy documentary films	Hoop Dreams, Roger & Me, Thin Blue Line, Crumb, Buena Vista Social Club, American Movie	Documentary	329
Fans of David Lynch films	Eraserhead, Blue Velvet, Wild at Heart, Lost Highway, Mulholland Dr., . . . (8 total)	—	176
Fans of 1970s New Hollywood auteur films	Chinatown, Taxi Driver, Godfather, Godfather: Part II, Nashville, . . . (16 total)	—	1787
Fans of 1980s slasher horror films	Halloween, Friday the 13th, Nightmare on Elm Street, Prom Night, Terror Train, . . . (11 total)	Horror	583
Fans of classic 1930s–40s screwball comedies	Bringing Up Baby, It Happened One Night, His Girl Friday, Philadelphia Story, My Man Godfrey, . . . (14 total)	Comedy	432
Fans of French New Wave cinema	Breathless, 400 Blows, Jules and Jim, Contempt, Band of Outsiders, . . . (12 total)	—	47
Fans of pre-1960 film noir	Double Indemnity, Maltese Falcon, Out of the Past, Big Sleep, Sunset Blvd, . . . (15 total)	Film-Noir	540
Viewers of silent-era cinema	Metropolis, General, Gold Rush, City Lights, Nosferatu, . . . (11 total)	—	230
Fans of classic Japanese samurai cinema	Seven Samurai, Yojimbo, Sanjuro, Throne of Blood, Ran, . . . (10 total)	—	1724

Continued on next page.

Table 13 (continued)

Query	Title patterns (representative)	Genre	n_+
Fans of Italian neorealism and post-war Italian cinema	Bicycle Thief, La Dolce Vita, 8 1/2, La Strada, Umberto D, ... (11 total)	—	60

Paired Wilcoxon p-values for MovieLens retrieval are consolidated in Appendix D, Table 10, alongside the Open e-commerce and audience-characterization tests. The headline conclusions for MovieLens: SAE and K-Means encoding are statistically indistinguishable on Lift@n_{pos} and AUROC. SAE wins Coverage by a large and highly significant margin on both encoders. SAE beats the text-embedding baseline on Lift but is nominally tied on AUROC, consistent with the text baseline's dense-by-construction coverage giving it a full-population comparison set. The $\text{AUROC}_{\text{scored}}$ column of Table 2 restricts to users each method actually scored, which leaves the text baseline slightly ahead on this metric.

E.3 Held-out demographic labels

Because MovieLens ground truth is derived from titles, which the auto-interpretation prompt also shows, retrieval could in principle reflect LLM title matching rather than the decomposition. As a control, we retrieve against all 14 of MovieLens's self-reported demographic labels (age, gender, and occupation groups), which no stage of the pipeline sees, changing nothing else. The SAE reaches AUROC 0.58 (SASRec) and 0.60 (BERT4Rec) and Lift 2.00 and 2.06, against AUROC 0.54 and Lift 1.28 for the text-embedding baseline (one-sided paired Wilcoxon on AUROC over query and seed, $p \leq 3\times10^{-4}$). K-Means encoding also exceeds the text baseline, so the effect reflects sparse decomposition rather than our SAE specifically. If the benchmark measured title matching, both methods would degrade together. Instead, only the method that depends on item text does.

E.4 Sensitivity to the confidence threshold

The auto-interpretation confidence filter (≥ 0.6, cf. Section 3.2) removes about a third of SAE features on MovieLens but only a tenth of K-Means features, because the LLM assigns the broader K-Means features higher confidence. Table 14 re-runs retrieval at thresholds from 0.0 (no filter) to 0.7. Across this range, the Lift and AUROC differences between the SAE and K-Means encoding stay small, and the SAE maintains its advantage in coverage, which grows with the threshold. The threshold therefore acts as a resolution parameter rather than a tuned setting.

Table 14: Sensitivity of MovieLens retrieval to the auto-interpretation confidence threshold (operating point 0.6). SAE minus K-Means encoding: Lift as a percentage of the K-Means value, AUROC and $\text{AUROC}_{\text{scored}}$ as absolute differences, and coverage as the raw SAE / K-Means pair. Computed over 3 SAE seeds per encoder, a different seed set from Table 2, so the 0.6 row differs slightly from it.

Encoder	Threshold	ΔLift	ΔAUROC	$\Delta\text{AUROC}_{\text{scored}}$	Coverage (SAE / K-Means)
SASRec	0.0	+6.3%	−0.016	−0.004	0.973 / 0.818
	0.5	+10.8%	+0.000	+0.011	0.976 / 0.817
	0.6	+11.2%	+0.009	+0.018	0.975 / 0.808
	0.7	+7.4%	+0.019	+0.019	0.983 / 0.795
BERT4Rec	0.0	−5.8%	−0.019	+0.003	0.971 / 0.847
	0.5	−4.2%	−0.016	+0.006	0.973 / 0.846
	0.6	−2.9%	−0.009	+0.013	0.979 / 0.843
	0.7	−4.3%	−0.006	+0.012	0.979 / 0.828

E.5 Audience characterization: protocol and statistics

We evaluate at matched k=5 feature budget and a 10% top-activator threshold per feature (matching the auto-interpretation sampling convention) on 20 franchise-level audiences in MovieLens-1M (≥ 2 franchise films per user, ≥ 30 users per audience). The K-Means-encoding reference is thresholded to match the SAE's mean L_0, following Section 5.

Top-k diversity. Per audience, we rank features by lift and compute top-k *redundancy* as the median pairwise cosine between BGE-large-en-v1.5 [Xiao et al., 2023] embeddings of the top-k features' {feature_name, feature_description} strings (lower cosine = less redundant, more diverse). We use BGE rather than the retrieval-standard MiniLM here because BGE provides finer paraphrase-discrimination needed for this metric, which specifically targets near-paraphrases that retrieval-tuned encoders collapse by design. The SAE decomposition yields a significantly less redundant top-5 than K-Means encoding on both encoders (SASRec K-Means $-$ SAE median cosine Δ=0.066, p=0.002; BERT4Rec Δ=0.032, p=0.049; Stouffer $p\approx 4\times 10^{-4}$, one-sided paired Wilcoxon with alternative K-Means>SAE, across 20 audiences).

Reverse-selector audience coverage. To probe whether redundancy costs audience coverage rather than being a free diversity bonus, we reverse the feature selector: we rank features by on-topic cosine similarity between their {name, description} and an LLM-generated audience description, take the top-5, then measure the fraction of each audience's top-activators covered by the selected top-5. The SAE top-5 covers significantly more of the target audience (SASRec Δ=0.011, p=0.0003; BERT4Rec Δ=0.017, p=0.0001; Stouffer $p\approx 10^{-7}$). The K-Means-encoding reference has higher per-feature lift but narrower per-feature activation distributions, so its redundant top-5 does not translate into better audience coverage. The SAE's L1-sparsity and overcomplete dictionary produce a decomposition in which each selected direction contributes a distinct explanation of behavior — the property this task actually rewards.

Feature-level redundancy diagnostic. The top-k-diversity effect above has a feature-level structural account. For each of the 10 curated niche audiences in Appendix E.2 with $n_{\text{positive}} \leq 500$, we identify SAE and K-Means features whose top-50 activators overlap the audience's positive set (Jaccard$\geq$0.05) and whose LLM interpretation confidence is $\geq$0.6 (matching the retrieval pipeline's filter). Among these features, we compute pairwise activation Pearson correlation and an effective-concept count by agglomerative clustering at correlation threshold 0.5. The redundancy ratio is features per effective concept. Across the 5 niche audiences where both methods have $\geq$2 confidence-passing matched features (documentary, David Lynch, 1930s–40s screwball, French New Wave, Italian neorealism), SAE has mean activation correlation 0.16 vs K-Means 0.29, and a redundancy ratio of 1.00 vs 2.20. K-Means features that surface a single audience decompose into 2–4 redundant partitions per effective concept; SAE features are structurally distinct even when multiple features co-surface the same audience.

Open e-commerce feature-level redundancy. Applying the same diagnostic to the SVD-on-counts SAE, with category audiences as ground truth and a precision-$\geq$ 0.70 match criterion (audience sizes of 300–2200 make Jaccard-based matching saturate at low values), we find the effect becomes more pronounced: SAE mean activation correlation 0.09 vs K-Means 0.33, redundancy ratio 1.14 vs 2.82 across 4/7 audiences with $\geq$2 matched features per method. 93% of active SAE features pass the confidence filter (vs 65% on MovieLens), consistent with the cleaner mode-to-feature alignment predicted for linear embedding functions in Section 3.1.

E.6 Volume-axis relabeling

A sparse decomposition of sequence-encoder embeddings can produce features that track engagement *intensity* (total films watched, recency of activity) rather than any taste pattern. Because such features fire on users with high activity regardless of content preference, they inflate retrieval lift on any audience query that correlates with engagement volume — for example, broad "fans of Hollywood films" queries where the positive set is dominated by heavy watchers.

We identify these features via a length-matched taste-free control: for each feature, we compare the content profile of its top activators against a group of non-activating users whose viewing counts match the activators' volume distribution. A feature is classified as *pure volume* if the content profiles are statistically indistinguishable (no genre or era is significantly enriched in the activator group relative to the length-matched control at p<0.05 after multiple-testing correction). Pure-volume features are relabeled from their auto-interpreted name to a single engagement-axis label ("heavy-watcher engagement axis") before retrieval. The same detection procedure is applied to SAE and K-Means-encoding codes, ensuring both methods receive the same treatment.

Relabeled engagement features contribute to retrieval only to the extent that the LLM selects them based on semantic match to the query text. The protocol therefore ensures that broad audience queries correlated with viewing volume are not spuriously boosted by engagement features; the features remain available in the dictionary but are interpreted honestly as an engagement axis rather than a taste.

F Auto-interpretation and retrieval prompts

This section lists the LLM prompt templates used at each stage of the pipeline. We use Claude Sonnet 4.6 for feature interpretation (the offline, one-time auto-interp stage) and Claude Haiku 4.5 for query-time feature scoring. The key prompt elements of each stage are summarized below.

F.1 Feature interpretation (auto-interp)

For each SAE / baseline latent, we sample 10 top-activating users (positives) and 10 random non-activating users (negatives). For Open e-commerce we show per-window purchase-category summaries; for MovieLens we show a structured per-user behavioral summary (separately cached; see Appendix F.2 for the summary prompt used). The interpretation prompt varies by dataset to match what the underlying embedding can encode:

Open e-commerce (categories mode, SVD-on-counts embeddings). The prompt instructs the model that the embedding is a TF-IDF-weighted SVD of user-by-category purchase counts in 6-month windows, and therefore encodes only which categories a user bought and roughly how often. It forbids brand-, title-, price-, or cadence-level claims, since the SAE cannot see them. The model is asked to infer *who these people are* (life-stage / lifestyle / household persona) from category combinations, at a granularity matched to the feature's sparsity (common features $\rightarrow$ broader personas; rare features $\rightarrow$ specific personas). Output is a JSON object with `feature_name`, `feature_description`, `confidence_score`, and per-pattern reasoning. An enrichment context precomputed over the top-activating users' windows (top categories with lift $> 2\times$ vs. population) is supplied alongside the per-window examples to anchor the LLM on population-distinctive categories.

MovieLens (titles mode, transformer embeddings). The prompt instructs the model that each positive is a user's behavioral summary computed from their viewing history. The model is asked to identify the specific taste pattern that distinguishes positives from negatives, drawing on title semantics, genre mix, era, and co-viewing patterns that the sequence encoder can encode. Output is the same JSON schema.

Key design choices: (i) system prompt forbids hallucinated attributes for the embedding modality, (ii) positives and negatives are presented with matched formatting so the model cannot detect class via superficial cues, (iii) confidence scores below 0.6 are excluded from downstream retrieval.

F.2 MovieLens behavioral-summary prompt

Before auto-interpretation, each MovieLens user is summarized via a one-shot LLM call (Claude Sonnet 4.6) on their chronological watch history. The summary is cached per user and reused across all SAE / baseline auto-interp passes.

System prompt. "You are a careful analyst producing structured behavioral summaries from movie watching histories. Base all claims only on the data shown. Do not invent patterns the history does not support."

User prompt. Per-user, the prompt supplies the chronologically ordered watch history (up to 150 items; title + release year + genres), basic stats (total count, earliest/latest release year), and instructs the model to produce six terse sections: (i) *Volume and engagement* (HEAVY/MODERATE/CASUAL classification against a 150-film MovieLens median), (ii) *Era profile* (decade-level release-year distribution with approximate fractions), (iii) *Genre profile* (top 5–7 genres with fractions), (iv) *Stylistic/thematic tendencies* (2–5 specific patterns, avoiding vague labels), (v) *Director/franchise affinity* (directors with $\geq$3 films or clear franchise patterns), (vi) *Avoidances* (genres/eras notably absent). The

prompt explicitly forbids the model from inferring time-viewing rates or absolute viewing dates, since MovieLens does not include viewing timestamps and release years only bracket the films themselves.

F.3 Query-time feature scoring

Given an NL audience query, the retrieval pipeline asks the LLM to score each interpreted feature's relevance to the query on a 0–10 scale. The prompt shows the query and a batch of `{feature_name, feature_description}` pairs; the model returns a score per feature and optionally a brief rationale. Features scoring ≥ 5 are retained; the retained features' activations are weighted by a sharpened cosine similarity between the feature text and the query (using `all-MiniLM-L6-v2` sentence embeddings) combined with the LLM score, capped at 50 features per query, and summed per user. This is the "weighted sum of activations on retained features" described in Section 5.

The weighted-sum combinator is itself compositional: each audience query is answered by combining contributions from multiple LLM-selected features rather than any single one, which is what allows the pipeline to cover both broad audiences (e.g., genre-level) and niche audiences (e.g., era $\times$ sub-genre) without per-query structural changes.